forests

MDPI

Article

Ecological Gate Water Control and Its Influence on Surface Water Dynamics and Vegetation Restoration: A Case Study from the Middle Reaches of the Tarim River

Jie Wu [1,2,3], Fan Gao [1,2,*], Bing He [1,2], Fangyu Sheng [1,2,3], Hailiang Xu [1,3,*], Kun Liu [1,2,3] and Qin Zhang [1,2,3]

[1] College of Hydraulic and Civil Engineering, Xinjiang Agricultural University, Urumqi 830052, China; wj01243433@163.com (J.W.); bing_touch_he@163.com (B.H.); 13361140530@163.com (F.S.); lklyk1996@163.com (K.L.); zqin28@outlook.com (Q.Z.)
[2] Xinjiang Key Laboratory of Hydraulic Engineering Security and Water Disasters Prevention, Urumqi 830052, China
[3] State Key Laboratory of Desert and Oasis Ecology, Xinjiang Institute of Ecology and Geography, Chinese Academy of Sciences, Urumqi 830011, China
* Correspondence: gutongfan0202@163.com (F.G.); xuhl2024@163.com (H.X.)

Abstract: Ecological sluices were constructed along the Tarim River to supplement the ecosystem's water supply. However, the impact of water regulation by these sluices on the surface water area (SWA) and its relationship with the vegetation response remain unclear. To increase the efficiency of ecological water use, it is crucial to study the response of SWA to water control by the ecological gates and its relationship with vegetation restoration. We utilized the Google Earth Engine (GEE) cloud platform, which integrates Landsat-5/7/8 satellite imagery and employs methods such as automated waterbody extraction via mixed index rule sets, field investigation data, Sen + MK trend analysis, mutation analysis, and correlation analysis. Through these techniques, the spatiotemporal variations in SWA in the middle reaches of the Tarim River (MROTR) from 1990–2022 were analyzed, along with the relationships between these variations and vegetation restoration. From 1990–2022, the SWA in the MROTR showed an increasing trend, with an average annual growth rate of 12.47 km^2 per year. After the implementation of ecological gates water regulations, the SWA significantly increased, with an average annual growth rate of 28.8 km^2 per year, while the ineffective overflow within 8 km of the riverbank notably decreased. The NDVI in the MROTR exhibited an upward trend, with a significant increase in vegetation on the northern bank after ecological sluice water regulation. This intervention also mitigated the downward trend of the medium and high vegetation coverage types. The SWA showed a highly significant negative correlation with low-coverage vegetation within a 5-km range of the river channel in the same year and a significant positive correlation with high-coverage vegetation within a 15-km range. The lag effect of SWA influenced the growth of medium- and high-coverage vegetation. These findings demonstrated that the large increase in SWA induced by ecological gate water regulation positively impacted vegetation restoration. This study provides a scientific basis for water resource regulation and vegetation restoration in arid regions globally.

Keywords: ecological sluice regulation; surface water area; vegetation restoration; Google Earth Engine (GEE); Tarim River; arid region water management

Citation: Wu, J.; Gao, F.; He, B.; Sheng, F.; Xu, H.; Liu, K.; Zhang, Q. Ecological Gate Water Control and Its Influence on Surface Water Dynamics and Vegetation Restoration: A Case Study from the Middle Reaches of the Tarim River. *Forests* **2024**, *15*, 2005. https://doi.org/10.3390/f15112005

Academic Editor: Guntis Brūmelis

Received: 12 October 2024
Revised: 31 October 2024
Accepted: 5 November 2024
Published: 14 November 2024

1. Introduction

Water resources are the most critical ecological factor in arid and semi-arid regions and affect plant community growth and succession [1]. In these areas, surface water and groundwater from river systems serve as the primary water sources for natural vegetation [2]. Surface water bodies, including natural lakes, ponds, rivers, and artificial reservoirs and channels, are especially vital in arid inland areas, where they play a crucial role in maintaining terrestrial ecosystem stability and supporting sustainable socioeconomic development [3]. However, climate change and human activities have disrupted the original

distribution of surface water [4], leading to an ecological imbalance in water supply and demand, as well as the degradation of desert riparian vegetation in certain regions [5]. Consequently, the rational management of water resources using riparian ecological hydraulic projects has attracted considerable focus from scientific communities both domestically and internationally.

As remote sensing technology and geographic information systems (GIS) have rapidly progressed, optical remote sensing data have become a major information source for monitoring large-scale surface water dynamics due to their ease of access, ease of processing, and high accuracy in waterbody extraction [6]. For instance, the threshold method examines the spectral properties of aquatic bodies and selects suitable thresholds to effectively distinguish them [7]. The water index method, in contrast, utilizes the differences in reflectance between the blue–green and infrared bands to generate characteristic indices that amplify information about water bodies, thus facilitating water extraction. The Normalized Difference Water Index (NDWI), which utilizes green and near-infrared bands from Landsat data to enhance water features, was initially proposed by S.K. McFeeters [8]. Subsequently, H Xu subsequently improved this index by proposing the Modified Normalized Difference Water Index (MNDWI), which significantly increases water extraction accuracy in urban areas [9]. Furthermore, Zou et al. developed a rule set for automated water extraction by integrating the MNDWI, NDVI, and EVI [10]. This rule set does not require a threshold for the MNDWI and has proven to be more effective in extracting wetland water bodies. It has been widely applied on a global and intercontinental scale [11]. In recent years, the powerful interaction and computational capabilities of GEE have overcome the limitations of traditional remote sensing techniques in handling long time series and large-scale spatial data, which makes GEE an efficient tool in waterbody research [12,13]. It has become an efficient tool in the field of waterbody research [14,15]. For example, Pekel et al. used the GEE platform to produce global surface water change remote sensing products on annual and monthly scales from 1984 to 2020. They provided 30-m spatial resolution global dynamic waterbody information that covers the temporal and spatial distribution, change intensity, transformation, regeneration cycles, and characteristics of seasonal and permanent water bodies [16]. Zou et al. processed 370,000 images of data from the GEE cloud platform to extract data on open water areas within the United States and analyze its changing trends and causes [17].

To restore the riparian forest ecosystems of the Tarim River Basin, the Chinese government invested 10.7 billion yuan in comprehensive management and conservation efforts in 2000 [18]. Several key ecological measures involved increasing water flow in the downstream river sections, constructing ecological water diversion dams in the flood-prone middle reaches, and distributing ecological gates along the dams. Ecological water diversion plays a crucial role in restoring degraded ecosystems in arid and semi-arid regions. It supplies essential water replenishment to damaged ecosystems through the strategic introduction of water sources [19,20]. The widespread distribution of ecological gates is critical for achieving ecological regulation and precise regional division in the Tarim River Basin [21]. However, uncertainties and inconsistencies exist in the scale and spatial distribution of water diversion [22], posing challenges to the scientific assessment and policy formulation of ecological water diversion projects. The remote sensing satellite monitoring of hydrological changes and use of vegetation indices to identify changes in vegetation density and greenness have been widely applied [23–25]. By analyzing the impact of surface hydrology on vegetation, an in-depth study of the effects of ecological sluice water transfers on vegetation can be used to comprehensively assess the ecological benefits of ecological water transfer projects in the Tarim River Basin [26].

Previous studies have determined the degree of ecological restoration and the comprehensive benefits of ecological water diversion based on factors such as the physiological growth of *P. euphratica*, vegetation remote sensing, and groundwater monitoring [19,27]. However, research on the distribution patterns of surface water bodies and the relationship between the vegetation response and gate-controlled water regulation remains limited.

Therefore, this study selected the middle reaches of the Tarim River (from Yingbazha to Qiala) as the research area. Using GEE cloud platform technology and integrating Landsat-5/7/8 satellite imagery, this study comprehensively utilized a mixed index rule set for automatic waterbody extraction combined with field investigation data to reveal the spatiotemporal dynamics of SWA and vegetation response characteristics over the past 33 years. This study quantitatively analyzed the spatiotemporal characteristics of surface water bodies and vegetation recovery responses before and after ecological gate control. The research findings address the knowledge gap concerning the effects of environmental water resource redistribution on vegetation dynamics and surface water availability through floodgate regulation. This study provides scientific evidence for the essential role of global water resource management in maintaining ecosystem health, especially in arid regions.

2. Materials and Methods

2.1. Study Location

The Tarim River is located along the northern edge of the Taklamakan Desert within the Tarim Basin and is the longest inland river in China, with a total length of 2137 km [20]. This study focuses on the middle reaches of the Tarim River that covers the section from Yingbazha to Qiala and spans a total length of 398 km. Protective embankments are present on both sides of the river, with widths ranging from 1 to 3 km (Figure 1). In 2000, the government constructed water diversion dams and ecological gates along the main channel, with 34 ecological gates built in the middle reaches of the Tarim River; construction was completed in 2009 [19]. The floodwaters during the flood season can be effectively converted into ecological water, supplying vegetation such as the *P. euphratica* forests along the Tarim River [26,28]. This region is characterized by an extremely arid continental warm climate, with sparse rainfall and high evaporation rates [29]. The average annual precipitation ranges between 18 and 45 mm, while the average annual evaporation reaches between 2500 and 3000 mm. The main soil types include sandy soil, oasis meadow soil, meadow soil, and saline soil [25]. For this study, we segmented the area from Yingbazha to Qiala into four distinct sub-regions:

S1: Yingbazha to Shazihe,
S2: Shazihe to Wusiman,
S3: Wusiman to Arqike, and
S4: Arqike to Qiala.

2.2. Vegetation Response Monitoring Sample Strips and Sample Placement

We focused on the Kambaerwustan ecological gate irrigation area, which is a major supplementary water area for *P. euphratica* forests in the middle reaches of the Tarim River. The Kambaerwustan ecological gate irrigation area is located between Yingbazha and Shazihe, and it marks the starting point of the water conveyance dike on the northern bank of the middle reaches of the Tarim River. Analysis of the water discharge from the ecological gates over the past decade revealed substantial changes and responses in the Kambaerwustan ecological gate irrigation area, which makes it a typical monitoring area.

Monitoring transects and plots were established as follows. Beginning 150 m from the ecological gate, three replicate transects were set up. The river water could reach only approximately 600 m from the discharge point, so plots were arranged within this 600-m range. Tree plots, each sized 25 by 25 m, were established at 150-m intervals along each transect. Within each tree plot, two shrub plots, each measuring 5 by 5 m, and three herbaceous plots, each measuring 1 by 1 m, were randomly placed. A total of three monitoring transects and 12 tree monitoring plots were set up in the Kambaerwustan monitoring area of the middle reaches of the Tarim River (Figure 2).

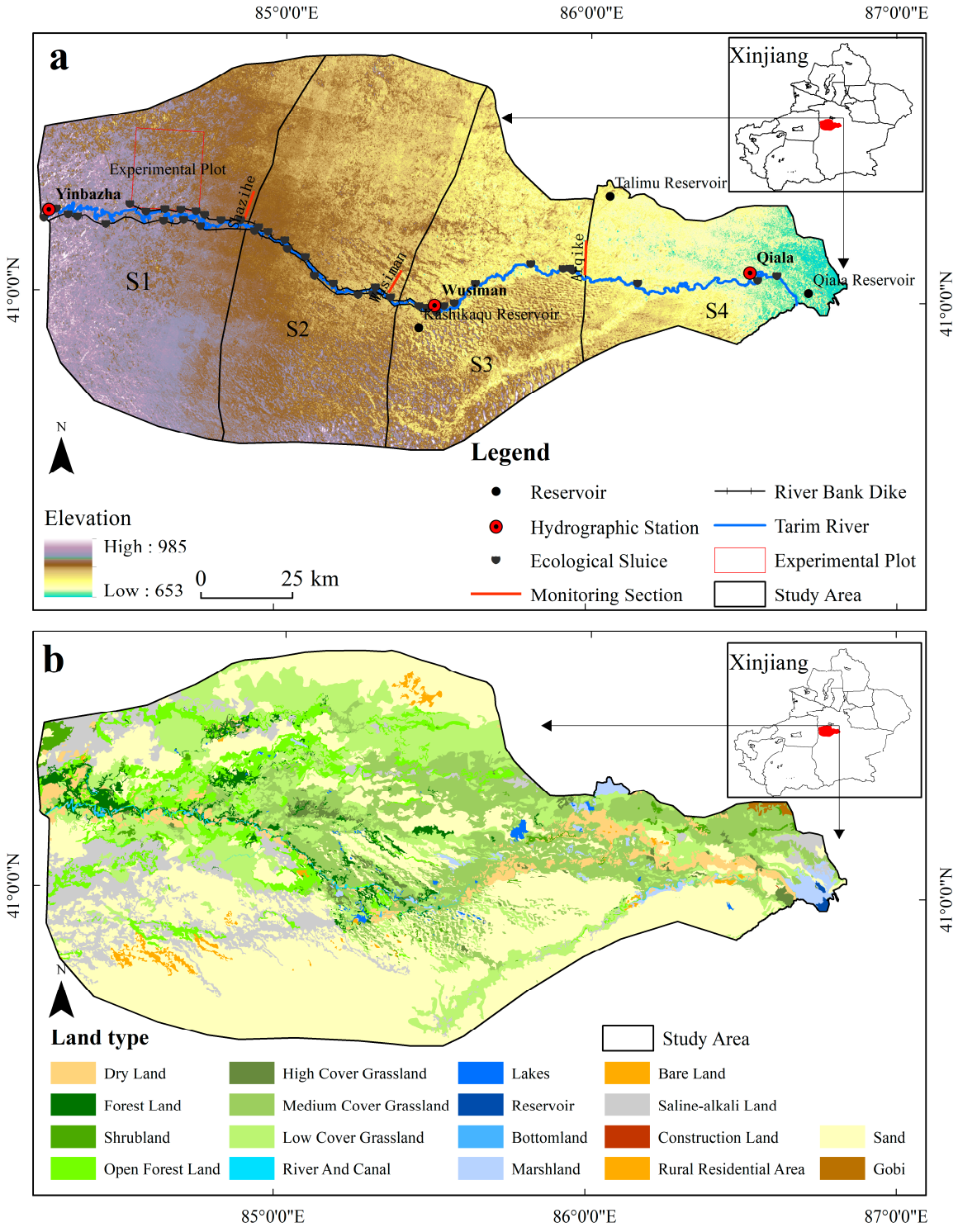

Figure 1. Map of the study area ((**a**). Elevation maps (**b**). 2020 Land use type maps).

The monitoring indicators included repeated monitoring of the three transects in June 2016, 2017, and 2018. The 2016 data served as the control group (before ecological water supplementation), while the 2017 and 2018 data were used as the experimental group. The sample survey method [30] was employed to investigate and statistically analyze the species in the experimental and control plots. The major indicators included the species composition of the *P. euphratica* community, the frequency and distribution of *P. euphratica* seedlings, the diameter at breast height (DBH) of mature *P. euphratica*, and the number of *P. euphratica* individuals per unit area.

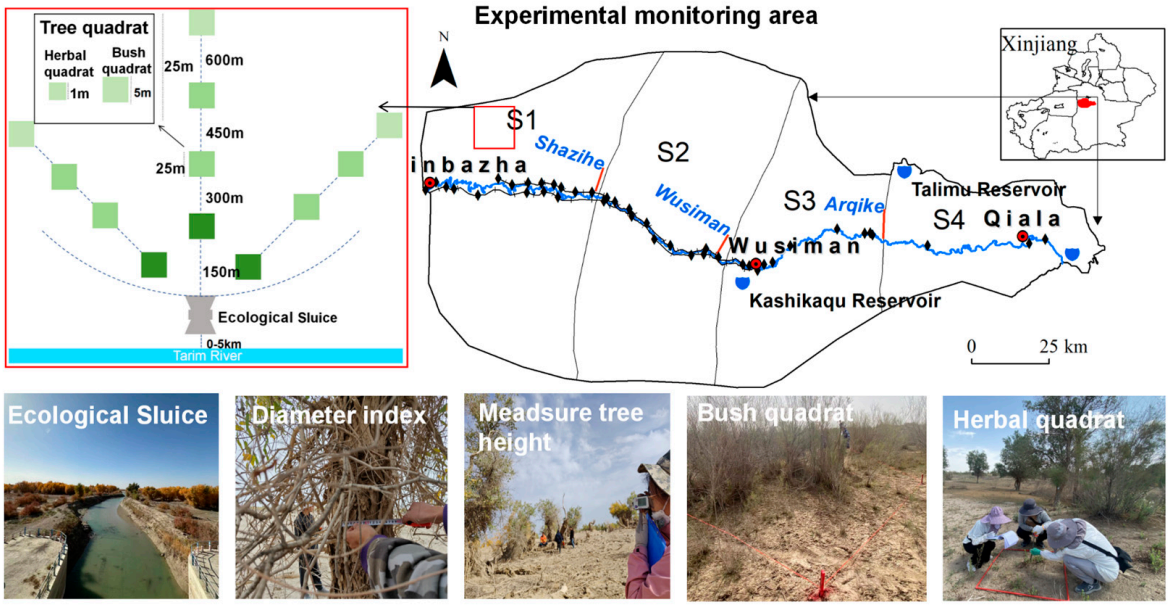

Figure 2. Schematic layout of the monitored sample plots in the study area.

2.3. Data Sources

Based on the GEE cloud platform (v0.1.350), this study processed original Landsat 5 TM (Developed through a collaboration involving NASA, NOAA, EOSAT, USGS, and GE, Santa Barbara, CA, USA), Landsat 7 ETM+ (Raytheon SBRS (Santa Barbara Remote Sensing), Goleta, CA, USA), and Landsat 8 OLI (Ball Aerospace & Technologies Corp., Boulder, CO, USA) images in batches. Data preprocessing included cloud and shadow masking to improve data quality. Following this, the annual average values of the NDVI and FVC were calculated for the study area to maintain temporal data stability, supporting a long-term analysis of vegetation dynamics. Additionally, Sentinel-2 data [31] was used for validation and comparison to assess the reliability of the Landsat-derived results. To ensure the accuracy of waterbody extraction, DEM data was used to remove mountain shadows that interfere with waterbody identification. The JRC Global Surface Water (GSW) data is employed to compare and validate the results of waterbody extraction. Specific data sources are provided in Table 1.

Table 1. Source of data.

Data	Time Period	Spatial Resolution	Time Resolution	Data Source
Landsat 5 TM	1990–2012	30 m	15 d	U.S. Geological Survey
Landsat 7 ETM+	1999–2002	30 m	15 d	U.S. Geological Survey
Landsat 8 OLI	2013–2020	30 m	15 d	U.S. Geological Survey
Sentinel-2MSI	2017–2020	10 m	10 d	European Space Agency
NASADEM	2020	30 m	—	NASA Jet Propulsion Laboratory
JRC GSW	1984–2022	30 m	—	European Commission Joint Research Centre

2.4. Study Methods

2.4.1. Water Extraction and Accuracy Verification

This study employs a hybrid index rule set for waterbody extraction, grounded in the algorithm developed by Zou et al. [17]. The Landsat satellite imagery data was preprocessed using JavaScript scripts on the GEE platform, which included cloud removal and the calculation of indices such as MNDWI [9], NDVI [32], and EVI [33]. The criteria for extracting waterbodies are defined as $MNDWI > NDVI$ or $MNDWI > EVI$, and $EVI < 0.1$.

This hybrid index method has been successfully employed in research conducted across various regions, including the northern slope of the Kunlun Mountains situated in an alpine region [34], the Yellow River Basin [10,35], the coastal areas of East Asia [36], and the Horqin Sandy Land [37]. These studies demonstrate that the hybrid indices possess significant applicability and accuracy in diverse ecological settings, effectively capturing changes in surface waterbodies. The formulas for these indices are presented below:

$$MNDWI = \frac{Green - SWIR}{Green + SWIR} \tag{1}$$

$$NDVI = \frac{NIR - Red}{NIR + Red} \tag{2}$$

$$EVI = 2.5 \times \frac{NIR - Red}{NIR + 6 \times Red - 7.5 \times Blue + 1} \tag{3}$$

where *Blue*, *Green*, *Red*, *NIR*, and *SWIR* represent the blue, green, red, near-infrared, and shortwave infrared bands of Landsat imagery, respectively.

The mixed spectral index method for waterbody extraction is still affected by mountain shadows. Shadows can cause variations in the spectral response of identical objects, leading to substantial deviations in water and vegetation index values within the same area. To mitigate the impact of shadows on NDVI, object-oriented methods are commonly employed to detect and adjust DN values in shadowed regions [38]. Alternatively, terrain-correction models are applied [39]. Given that waterbodies are mainly situated in flat terrains, numerous researchers have utilized terrain slope data to reduce the influence of shadows in mountainous regions across various images [40]. This study adopted previous research findings [41] to improve the extraction results by setting a rule that eliminates mountain shadows in waterbodies when the slope is less than 8°. The method for calculating the Water Inundation Frequency (*WIF*) involves determining the ratio of the total number of times a waterbody is identified each year to the number of effective observations. Based on previous research [42], regions with 25% < $WIF \leq 75\%$ are defined as seasonal waterbodies, whereas regions with $WIF > 75\%$ are defined as permanent waterbodies. The formula for calculating *WIF* is presented as follows:

$$WIF = \frac{1}{N}\sum_{i=1}^{N} w \tag{4}$$

where N indicates the number of effective observations annually, while w is a binary variable representing the waterbody type at each pixel, with a value of 0 for nonwater bodies and 1 for waterbodies.

During the water transfer period from 2019 to 2022, this study employed Sentinel-2 MSI high-resolution imagery data, systematically collecting 715 samples encompassing various types of waterbodies, such as rivers, lakes, and reservoirs, as well as non-waterbody areas, to comprehensively validate the accuracy of the waterbody extraction results. Through classification analysis, 668 waterbody samples were identified, yielding an extraction accuracy of 93.76% and a Kappa coefficient of 0.86. The method demonstrates substantial classification accuracy and consistency in waterbody identification, underlining its applicability and reliability. To further increase the transparency of our findings, we conducted a comparative analysis of the extraction results with the JRC Global Surface Water (GSW) data set (Figure 3). The analysis demonstrates that our method provides more detailed information on waterbody distribution compared to the JRC data. This comparison offers a more comprehensive validation of the extraction results, enhancing the precision and reliability of detecting dynamic changes in waterbodies.

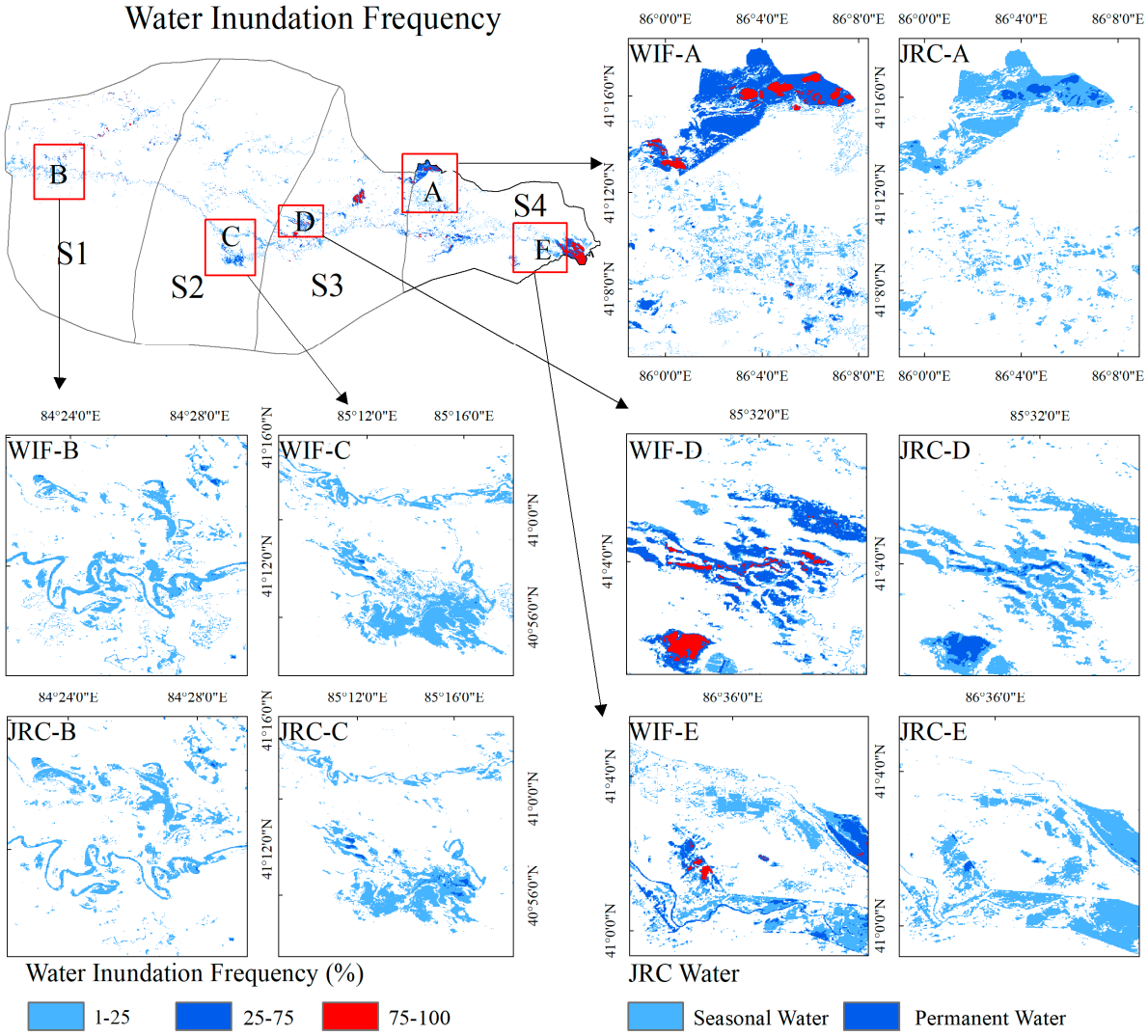

Figure 3. Comparison of waterbody extraction results with JRC data.

2.4.2. Extraction of the Intra-Annual Vegetation Characteristic Data

Based on the GEE platform, annual vegetation phenological indicators (start of season (SOS), and end of season (EOS)) were obtained with MODIS13Q1 EVI time-series data fitted with a double-logistic function (Equation (1)) [43].

$$f(t) = v_1 + v_2\left(\frac{1}{1+e^{(-m_1(t-n_1))}}\frac{1}{1+e^{(-m_2(t-n_2))}}\right) \quad (5)$$

where $f(t)$ is the fitted EVI value on day t; v_1 is the minimum fitted EVI for the year; v_2 is the difference between the maximum and minimum fitted EVI values for the year; and m_1, n_1, m_2, and n_2 are parameters representing the green-up and senescence stages of vegetation, with n_1 and n_2 indicating the dates that correspond to the maximum rates of green-up and senescence, respectively, and m_1 and m_2 identifying the slopes of the fitted curves.

The times that correspond to the maximum and minimum slopes of the fitted model curve represent the SOS and EOS, respectively, with the difference between them representing the growing season length (GSL) [44]. This method is adaptive and does not rely on subjective experience, which makes it suitable for the vegetation in the Tarim River Basin.

The double-logistic model based on the GEE platform demonstrated good stability across different land cover types. The fitted curves for different vegetation cover types (forest and cropland) differed greatly in the green-up and senescence stages. By measuring

the date when the EVI of a year reached the same magnitude as its long-term average value, the annual variability of forests and cropland could be determined.

2.4.3. Sen + MK Trend Analysis

The Theil–Sen median (TSM) trend analysis [45] and the Mann–Kendall (MK) nonparametric test are widely used methods for analyzing NDVI spatial variation characteristics [46]. This study combines these methods to assess the statistical significance of the Sen trend [47]. Compared to traditional univariate linear regression trend analysis [48], this integrated approach effectively mitigates the potential interference of data-distribution characteristics and missing data on research outcomes, while also reducing the impact of outliers [49]. The calculation formula is as follows:

$$\beta = \text{Median}(\frac{X_j - X_i}{j - i}), \forall j > i \quad (6)$$

where β represents the vegetation coverage trend. A positive β indicates an increasing trend, while a negative β indicates a decreasing trend. The function Median () represents the median.

The Mann–Kendall test is a nonparametric method for identifying trends in time series data. It does not require the data to conform to a normal distribution and is resilient in the presence of missing values and outliers. It is well-suited for evaluating the significance of trends in long-term time series data [50]. The calculation formula is detailed in the literature [51].

2.4.4. Mann–Kendall Mutation Analysis

To examine abrupt changes in the NDVI series from 2000 to 2022, the MK method was employed to test the time series. This method primarily detects changes in the variables from one relatively stable state to another. The calculation formula for the MK mutation test can be found in the literature [52].

2.4.5. Phased Development of Ecological Sluice Systems Along the Tarim River

The implementation of ecological sluices along the Tarim River was divided into three distinct phases. This division was guided by the timeline of dike construction and ecological water management interventions:

No Ecological Gate (NEG) Phase (1990–2000): During this period, no ecological sluice gates were in place.

Ecological Gate Construction (EGC) Phase (2000–2010): This phase marks the period focused on constructing ecological sluice gates along the riverbank, aiming to enhance water management and distribution to adjacent riparian zones.

Ecological Gate Control Water (EGCW) Phase (2010–2022): This phase corresponds to the operation and active control of water flow through the ecological gates, designed to enhance water availability for vegetation restoration and ecological stability.

2.4.6. Correlation Analysis

The Pearson correlation coefficient [53] was used to calculate the correlation between SWA data and FVC on a pixel-by-pixel basis, thus quantifying the relationship between FVC and SWA. The formula is as follows:

$$r = \frac{n(\sum xy) - (\sum x)(\sum y)}{\sqrt{[n\sum x^2 - (\sum x)^2][n\sum y^2 - (\sum y)^2]}} \quad (7)$$

where n is the sample size, and x and y represent the observed values of SWA and FVC, respectively.

3. Results

3.1. Spatiotemporal Dynamics of SWA in the Middle Reaches of the Tarim River

3.1.1. Temporal Dynamics in SWA of the MROTR

A comprehensive assessment of the SWA in the middle reaches of the Tarim River (MROTR) from 1990 to 2022 was conducted, including both permanent and seasonal water bodies, as well as their cumulative total. In this area, the total SWA increased from 79.36 km^2 in 1990 to 490.98 km^2 in 2022, which is an increase of 411.62 km^2, with an average annual growth rate of 12.47 km^2 per year (Figure 4). Specifically, in the non-ecological gate (NEG) phase, the growth of SWA was particularly notable, with an annual change rate reaching 20.5 km^2. This was largely due to substantial fluctuations in uncontrolled natural runoff that caused waterbody expansion. Between 2000 and 2010, as the EGC commenced, the SWA decreased to 87.73 km^2, with an average annual change rate of −16.88 km^2/year, reflecting instability in water resource management during the initial stages of ecological gate development. However, during the ecological gate-controlled water (EGCW) phase, the SWA increased rapidly, with an average annual growth rate of 28.8 km^2/year, particularly in the seasonal water area, which expanded at a rate of 11.86 km^2/year. This indicates the effectiveness of the ecological gates in regulating water resources.

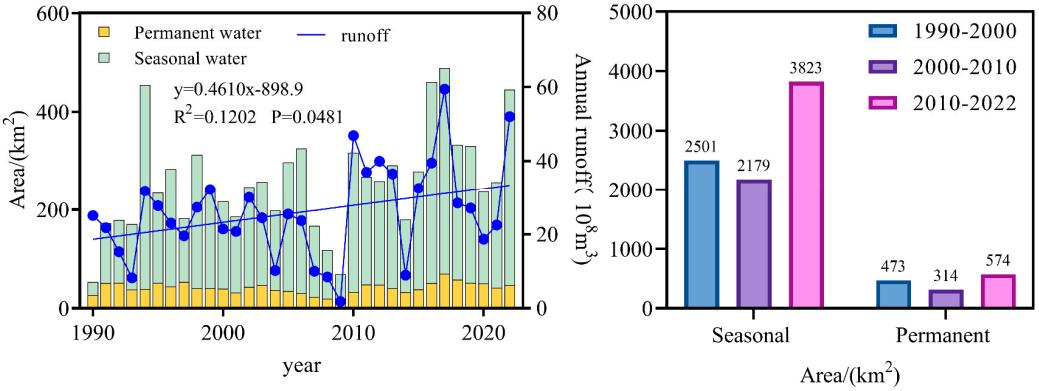

Figure 4. Time series of SWA in the MROTR, 1990–2022.

The permanent SWA remained relatively stable and fluctuated within a narrow range, whereas the seasonal SWA exhibited significant growth during the EGCW stage. The trends in SWA changes were consistent with the runoff data from hydrological stations in the MROTR, and the peak runoff years aligned with the expansion of the SWA. During the EGCW stage, the synchronization of peak runoff and seasonal water area expansion highlights the gates' efficiency in water regulation, particularly during peak flow periods. This regulation ensured an adequate water supply during the vegetation growth season, and it has created favorable conditions for the revival of riparian vegetation.

3.1.2. Spatial Changes in SWA of the MROTR

Using Geographic Information Systems (GIS) (ArcGIS 10.8), we compiled 33 images of water bodies captured between 1990 and 2022 to develop a comprehensive map illustrating the distribution of surface water over an extended period in the MROTR area (Figure 5a). Throughout the NEG period, the recorded maximum total area of water reached 2871 km^2. This area decreased to 2598 square kilometers during the EGC period. Nevertheless, in the EGCW period, there was a notable expansion in the total water area, reaching 4329 square kilometers. Most water bodies were located along the northern bank, with subregion S1 having the smallest proportion, accounting for 14.2% (Figure 5d), whereas S4 included the largest share at 36.6%. The average annual seasonal water areas for subregions S1 through S4 were determined to be 40.33 km^2, 56.04 km^2, 70.05 km^2, and 85.02 km^2, respectively (Figure 5b,c,e,f). The cumulative water areas were also calculated for each decade from 1990

to 2022 (Figure 5g). Throughout all phases, S4 consistently exhibited the largest cumulative water area, while S1 had the smallest.

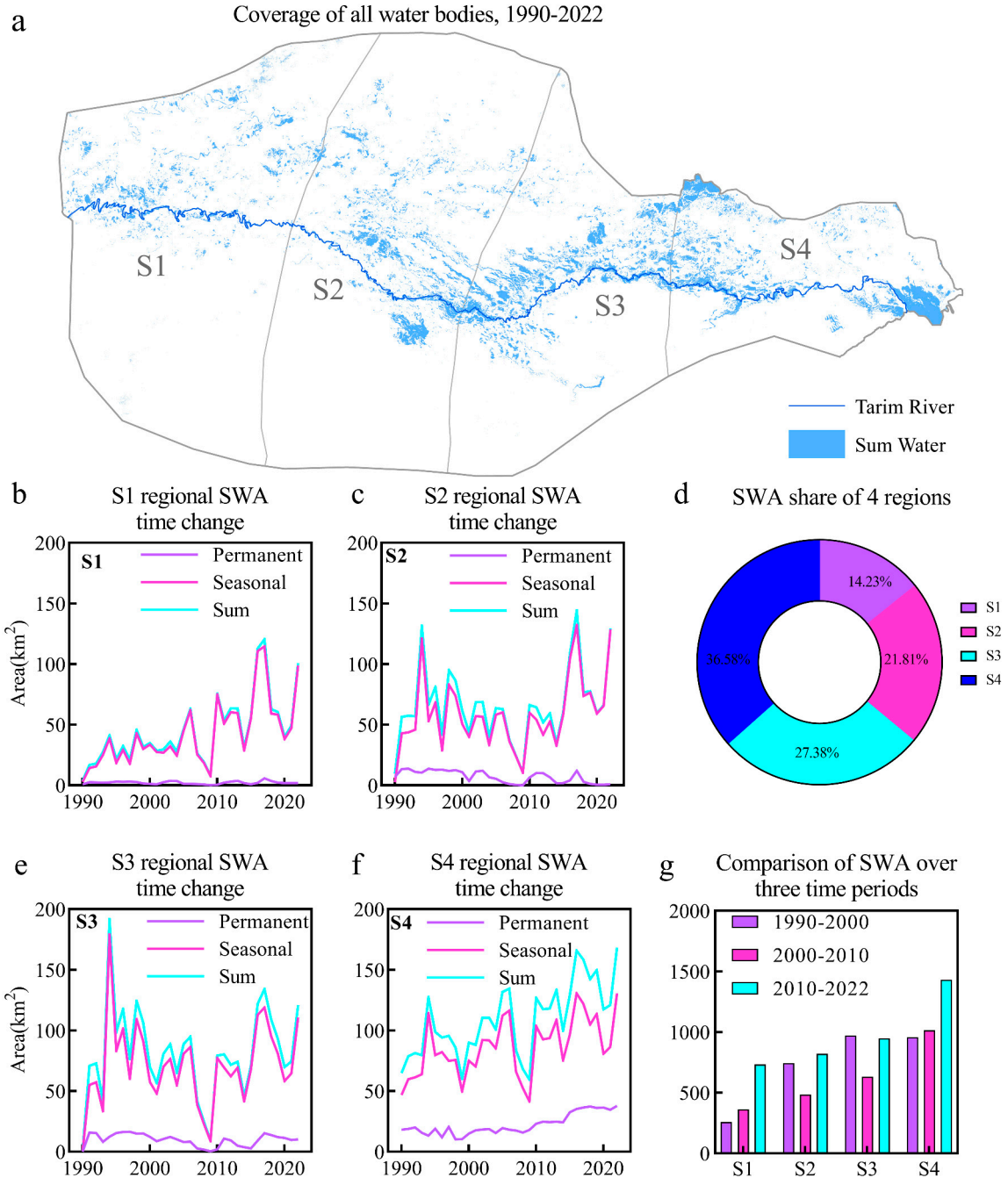

Figure 5. Sections S1–S4 SWA in the MROTR, 1990–2022. (**a**) Coverage of all water bodies,1990-2022. (**b**) Characteristics of temporal changes in SWA in the S1 region. (**c**) Characteristics of temporal changes in SWA in the S2 region. (**d**) S1–S4 regional SWA percentage. (**e**) Characteristics of temporal changes in SWA in the S3 region. (**f**) Characteristics of temporal changes in SWA in the S4 region. (**g**) Comparison of SWA over three time periods.

3.1.3. Dynamic Characteristics of the SWA Before and After the Control of Water by Ecological Sluice Gates

Each year's SWA was classified into four specific categories, namely, SWA < 200 km^2 (classified as dry years, SWA I), 200 km^2 < SWA < 300 km^2 (normal years, SWA II),

300 km^2 < SWA < 400 km^2 (wet years, SWA III), and SWA > 400 km^2 (extremely wet years, SWA IV), as detailed in Table 2.

Table 2. Annual SWA classification.

Level	Criteria for Division	Year
I	SWA < 200 km^2	1990, 1997, 2008, 2009
II	200 km^2 < SWA < 300 km^2	1991, 1992, 1993, 1995, 1997, 1999, 2000, 2001, 2002, 2003, 2004, 2012, 2014, 2020, 2021
III	300 km^2 < SWA < 400 km^2	1996, 1998 2005, 2006, 2010 2011, 2013, 2015, 2018, 2019
IV	SWA > 400 km^2	1994, 2016, 2017, 2022

To analyze the SWA during years with varying water inflows, representative years were selected. For the analysis of SWA, distinct years were selected across different levels: Level II included the years 1993, 2001, and 2014, while Level III encompassed 1996, 2005, 2013, 1998, 2006, and 2019. For Level IV assessment, 1994 and 2022 were the focal points.

GIS technology was utilized to create buffer zones at intervals of 1 km along the riverbanks extending from the ecological gates. This method facilitated the calculation of SWA for each segment of 1 km. The findings demonstrated variable changes in SWA at varying proximities to the riverbank before and after the implementation of the ecological gates (Figure 6). The data indicated that within the 2–8-km distance from the ecological gates, there was an average reduction in SWA of 4.7 km^2 per kilometer during the EGCW stage compared to the NEG stage. Similarly, SWA reduced by an average of 6.11 km^2 per kilometer during the EGC stage. During wet years, the average increase in SWA was 1.3 km^2 per kilometer in the EGCW phase within the 10–40-km range from the ecological gates compared to the NEG phase. This suggests that during wet conditions, the water control measures implemented by the ecological gates significantly enhance water distribution in remote areas. Similarly, in normal water years, the SWA in the EGCW stage increased by an average of 1.1 km^2 per kilometer within the 23–35-km range from the ecological gates, relative to the NEG phase. This further underscores the effectiveness of ecological gates in extending lateral water conveyance, even in relatively stable water conditions.

Since the implementation of the Tarim River embankment construction and the water regulation measures via ecological gates in 2010, ineffective water overflow within an 8-km radius has been effectively controlled, facilitating the lateral diffusion of water over long distances. In normal water years, the SWA expanded within the 23–35-km range. In wet years, water conveyance reached up to 38 km, markedly increasing the SWA from 10 to 40 km. During exceptionally wet years, the conveyance distance further extended to 40 km. These findings indicate that the establishment of ecological sluice and water-regulation measures have not only optimized the distribution of water resources near the riverbank but also significantly improved the efficiency and spatial coverage of long-distance water conveyance.

3.2. Characteristics of the Spatiotemporal Dynamics of Vegetation in the MROTR

3.2.1. Temporal Changes in Vegetation

Since 2001, the continuous development of water conveyance levees along with the installation of ecological gates in the MROTR has effectively minimized ineffective overflow, providing critical water sources for the vegetation on both banks. The water supply capacity of these gates is regulated according to the water requirements of the natural vegetation. The annual mean NDVI and the mean monthly NDVI from June to September for 2000 to 2022 were calculated (Figure 7a,b). The results indicated that among the four subregions (S1–S4), S4 had the highest NDVI values, with the annual mean NDVI following the order

S4 > S3 > S2 > S1. Furthermore, the NDVI in all subregions showed an upward trend. A trend analysis of the annual mean NDVI in the MROTR was conducted, and the results revealed that all four subregions passed the MK test for the period 2000–2022. Subregions S1, S2, and S4 exhibited increasing trends, with abrupt changes observed in S2 and S4 in 2005, which were associated with a significant reduction in SWA in the Tarim River from 2004 to 2005. In contrast, the S3 region experienced showed an abrupt change in 2019.

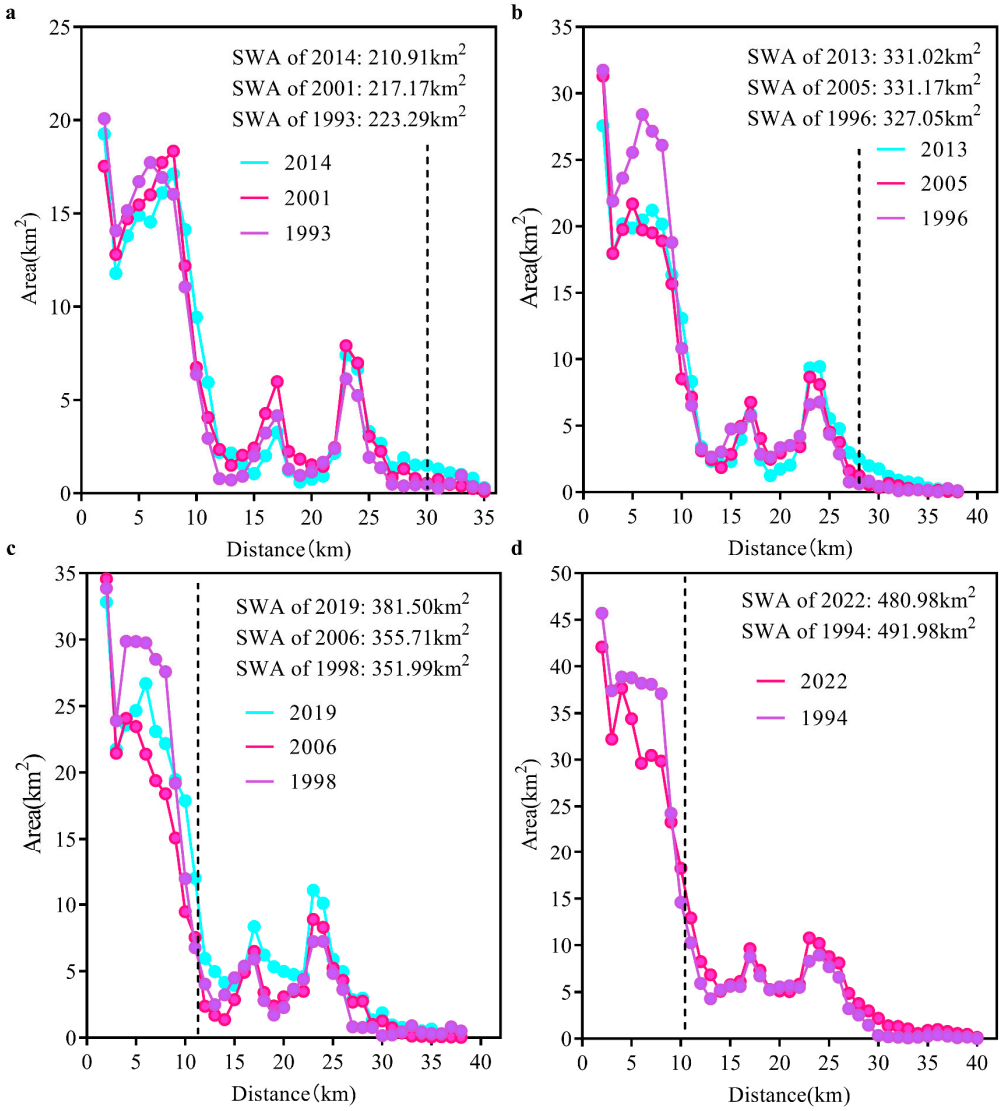

Figure 6. Changes in SWA at varying distances from the riverbank in different water volume years. (**a**) Change in SWA in a normal year. (**b**) Change in SWA in a wet year. (**c**) Change in SWA in a wet year. (**d**) Change in SWA in a extremely wet years year.

The statistics and change sequences for the SOS and EOS of the growing season in the four subregions from 2000 to 2022 are depicted in Figure 7c–f. The significance of the changes was weaker in the intra-annual indicators than in the interannual NDVI indicators, but the regional differences decreased. The MK test of the intra-annual characteristics of vegetation in the MROTR revealed that the SOS advanced in S1, S2, and S4. Abrupt changes occurred in 2006 for both S1 and S4 and in 2003 for S2. In the S3 region, an abrupt change occurred in 2004, with a trend toward a delayed growing season between 2006 and 2012. With respect to the EOS, abrupt changes were observed in 2007 for S1, S3, and S4, with the growing season end times beginning to delay in 2010, 2011, and 2008, respectively. The S2 region experienced an abrupt change in 2010, with an advancing trend in the growing

season end time from 2002 to 2013, followed by a delaying trend from 2014 to 2022. These findings indicate that ecological gate management has significantly impacted vegetation growth periods and has increased vegetation growth potential.

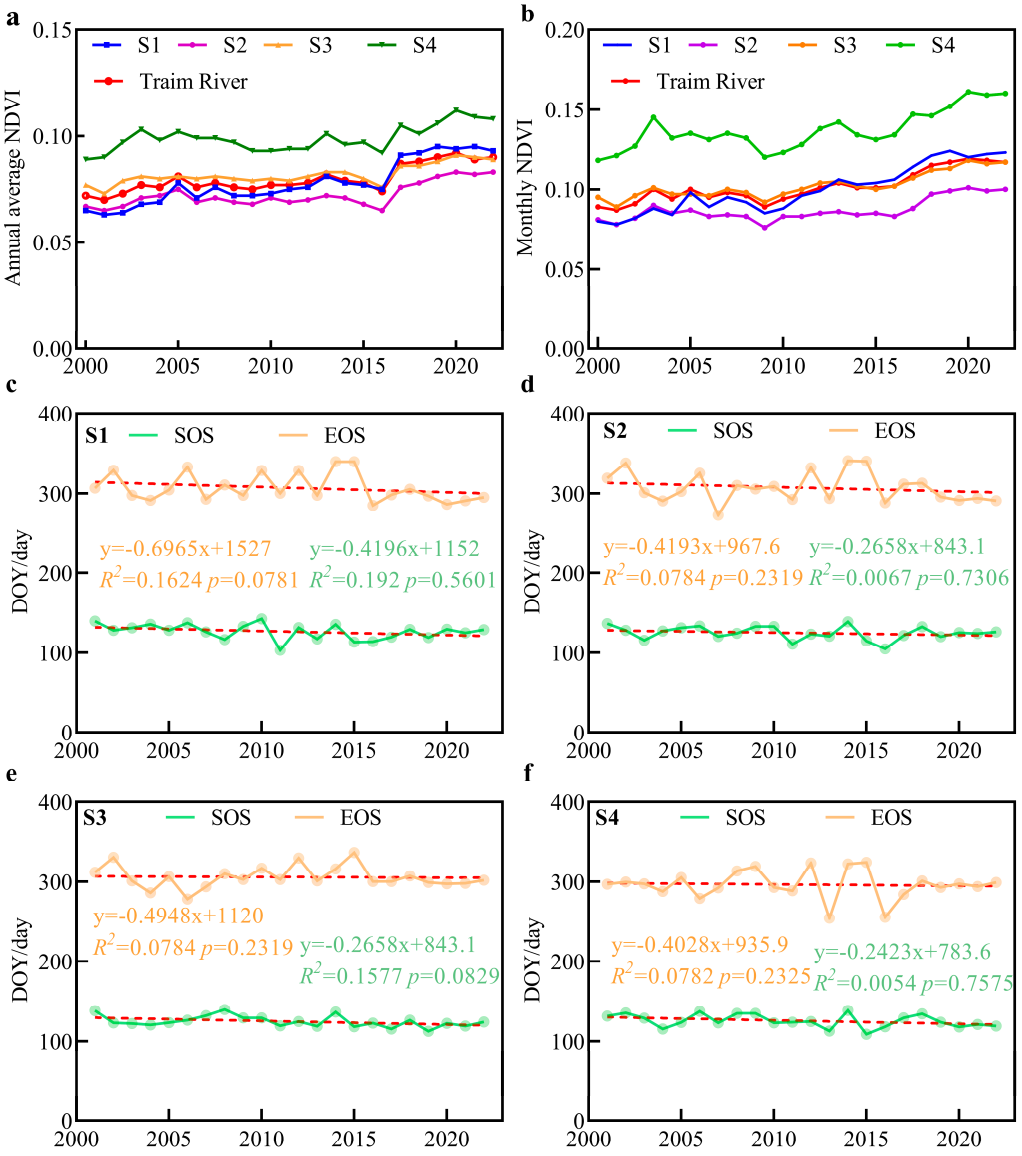

Figure 7. Time series of the interannual vegetation indicators of the MROTR, 2000–2022. (**a**). Annual mean NDVI (**b**). June–September monthly mean NDVI (**c**–**f**). Annual mean vegetation phenology.

3.2.2. Spatial Variation in Vegetation

From 1990 to 2022, the vegetation coverage exhibited a fluctuating downward trend (Figure 8) that was closely associated with the implementation of water regulation measures by the ecological gate system. During the NEG phase, the average high-coverage vegetation accounted for 22.67% of the total area. Following the construction of ecological gates in 2000, instability in early water regulation resulted in a reduction in the mean vegetation coverage, with the EGC phase showing a reduction in high-coverage vegetation to 21.21%. In the EGCW phase, from 2010 to 2022, high-coverage vegetation further decreased to 17.73%. Conversely, low-coverage vegetation gradually increased with water redistribution from 48.82% in 1990 to 56.21% in 2022.

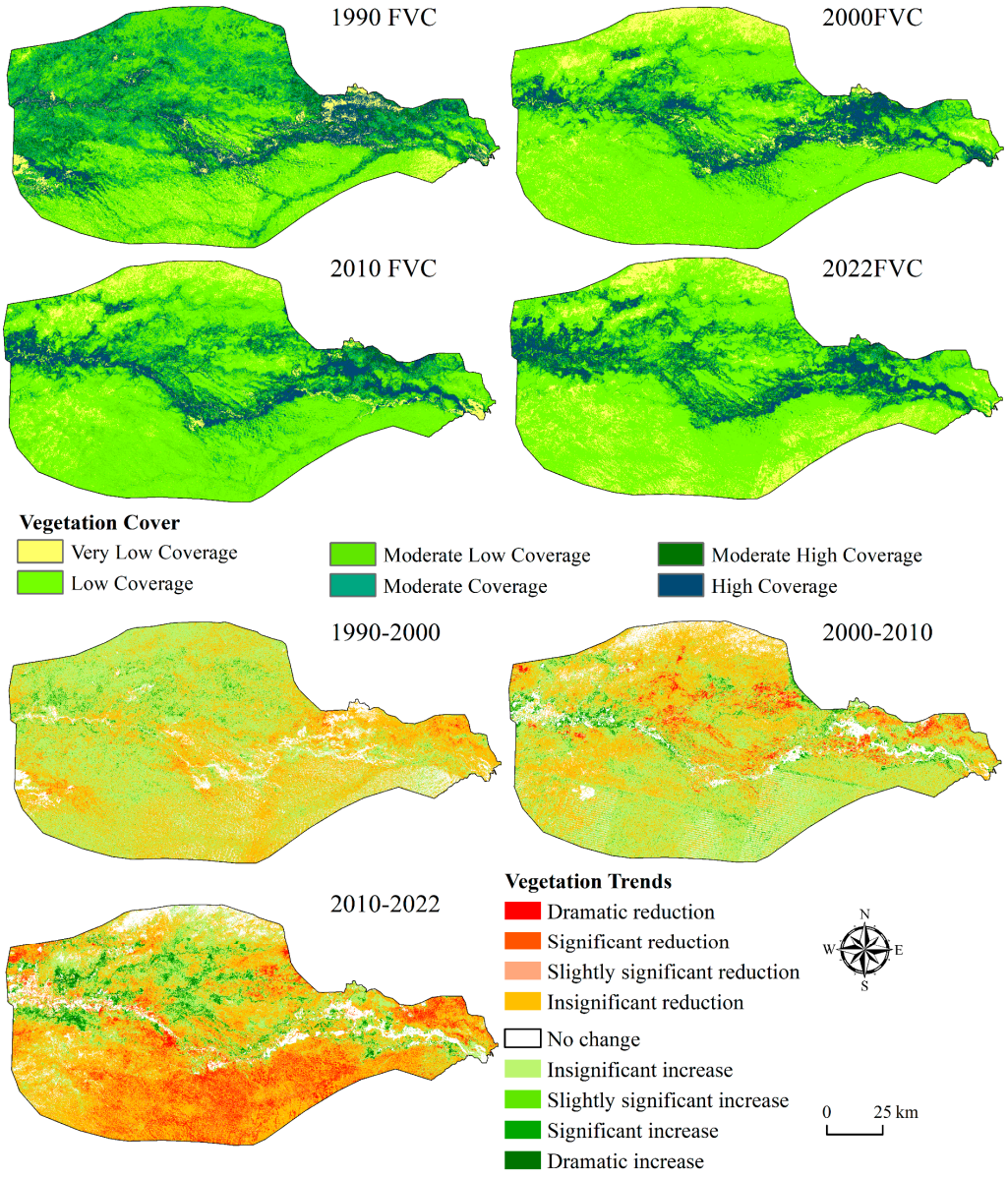

Figure 8. Spatial distribution and trends of the vegetation cover in the MROTR, 1990–2022.

The spatial distribution of vegetation coverage significantly changed after the construction of the ecological sluice and water regulation measures in 2000. According to the FVC change trend (Figure 8), from 2000 to 2010, there was a noticeable decrease in vegetation on the northern bank of the Tarim River, as the ecological gates had not yet fully come into effect. However, after the implementation of water control measures in 2010, the northern bank experienced a significant increase in water supply, leading to a substantial recovery of vegetation that accounted for 6.56% of the area with a significant increase in vegetation. In contrast, the vegetation on the southern bank significantly decreased, covering 19.69% of the area. Compared with the pregate phase, the postimplementation phase of the ecological gates had a differential impact on vegetation recovery. The northern bank experienced significant vegetation restoration, while the southern bank experienced a decline in vegetation coverage.

3.2.3. Characterization of the Vegetation Changes Before and After Water Control by Ecological Gates

The average vegetation cover during the NEG, EGC, and EGCW phases was calculated, along with the area of each vegetation cover type in 1-km increments within a 55-km

distance from the riverbank (Figure 9). Within 15 km of the riverbank, the area of low vegetation cover increased as the distance from the riverbank grew, but beyond 15 km, it gradually decreased. Between 1990 and 2022, the areas with low vegetation cover followed the order EGCW > EGC > NEG. For the other vegetation cover types, the area consistently decreased as the distance from the riverbank increased. The rates of increase and decrease in the vegetation cover area differed across vegetation types prior to and following the construction of the ecological gates. Further analysis was conducted to compare the vegetation cover area change rates between the NEG and EGC phases and between the EGC and EGCW phases. The results indicated that the increase in low vegetation cover was more pronounced during the EGC-EGCW phase than during the NEG-EGC phase. Conversely, the reduction in medium–low and high vegetation cover was less significant during the EGC-EGCW phase than during the NEG-EGC phase. These findings suggest that the implementation of water control at the ecological gates increased the area of low vegetation cover while mitigating the reduction trends for medium–low and high vegetation cover types.

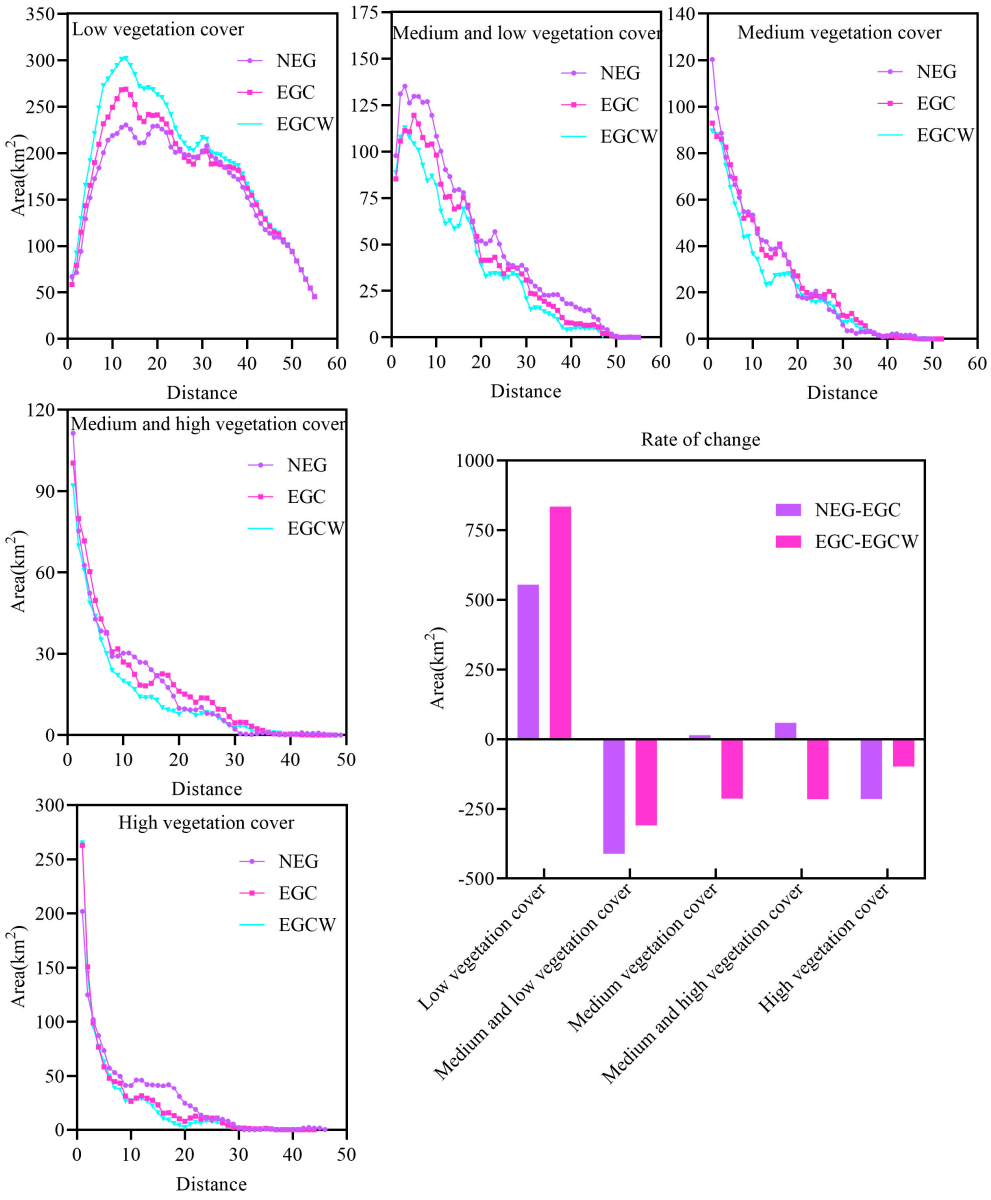

Figure 9. Area of each vegetation cover type at different stages before and after ecological gate control.

3.3. Response of Vegetation to Surface Water Area Changes in the MROTR

3.3.1. Monitoring Results of the Experimental Sample Points

In 2016, the government of the Xinjiang Uygur Autonomous Region launched an action to protect the source and upper MROTR and its *P. euphratica* forests by designating the upper and middle reaches as major pilot areas. From 2016 to 2018, we conducted field surveys in the middle reaches to quantitatively analyze the impact of surface water on the growth and diversity of desert riparian plant communities. In the middle reaches, 108 subplots of 1 m × 1 m were randomly set up within each larger *P. euphratica* plot near the Kanbaerwusitan ecological gate. The density of *P. euphratica* seedlings increased from 0.008 plants/m^2 in 2016 to 0.80 plants/m^2 in 2018, representing an increase of 0.72 plants/m^2 and a growth rate of 89.1%. These findings indicate that surface water strongly promotes the regeneration of *P. euphratica* plants.

In 2016, the occurrence frequencies of *P. euphratica* under excellent, good, medium, poor, and very poor growth conditions were 0.06, 0.17, 0.28, 0.31, and 0.172 plants/m^2, respectively. By 2018, these frequencies had changed to 0.11, 0.15, 0.34, 0.24, and 0.168 plants/m^2, respectively, with growth rates of 78%, −15%, 21%, −24%, and −3%, respectively. These changes indicate a shift in growth conditions toward better and medium grades, optimizing the growth structure of the *P. euphratica* forest.

Based on the field survey data from 2016 to 2018, the vegetation cover was monitored through remote sensing and compared for the same period. The SWA reached its maximum in 2017, with 510.29 km^2 in 2016, 557.98 km^2 in 2017, and 391.22 km^2 in 2018. Vegetation remote sensing monitoring areas were selected according to their distance from the riverbank to analyze the impact of SWA changes on vegetation. As shown in Figure 10, vegetation cover increased annually from 2016 to 2018, even though the surface water area significantly decreased in 2018 compared with 2017. High vegetation cover areas increased by 3% in 2018 compared with 2017, likely due to the increase in groundwater levels during the abundant water year of 2017, which continued to support vegetation growth despite the reduced water inflow in 2018.

3.3.2. Time-Lag Correlation Between Vegetation and the SWA

A comparative analysis of vegetation cover was conducted for the dry year of 2007 and the normal water years of 2011 and 2013, with SWAs measuring 189.2 km^2, 315.97 km^2, and 331.02 km^2, respectively. Despite the increase in SWA during these years, remote sensing data indicated a slight decrease in vegetation cover (Figure 11). A further investigation revealed a slight decline of the SWA values in the preceding years: 355.7 km^2 in 2006, 348.34 km^2 in 2010, and 305.46 km^2 in 2012.

To examine whether surface water has a lagged effect on vegetation cover in the MROTR, buffer zones were established at 0–5 km and 5–15 km from the river. The number of vegetation pixels in different coverage categories was extracted from these zones, and a correlation analysis was conducted with river inflow data, which determined the SWA for each year.

Within 5 km of the river, the correlation between river inflow and vegetation cover was assessed (Figure 12a1–a4). The results indicated that the correlation was stronger between river inflow and the subsequent year's vegetation cover than between river inflow and the same year's vegetation cover, with the coefficient of determination (R^2) improving by 0.1428, 0.0841, and 0.0411 for areas with no coverage, moderate coverage, and high coverage, respectively. In the 5–15 km buffer zone, similar patterns were observed (Figure 12c1–c4). The correlation between river inflow and the subsequent year's vegetation cover was again stronger, with the R^2 values increasing by 0.0929, 0.0993, and 0.0219 for areas with no coverage, moderate coverage, and high coverage, respectively. This indicates that vegetation within both 5 km and 5–15 km of the river exhibited a stronger response to the previous year's water conditions than to the current year's water levels.

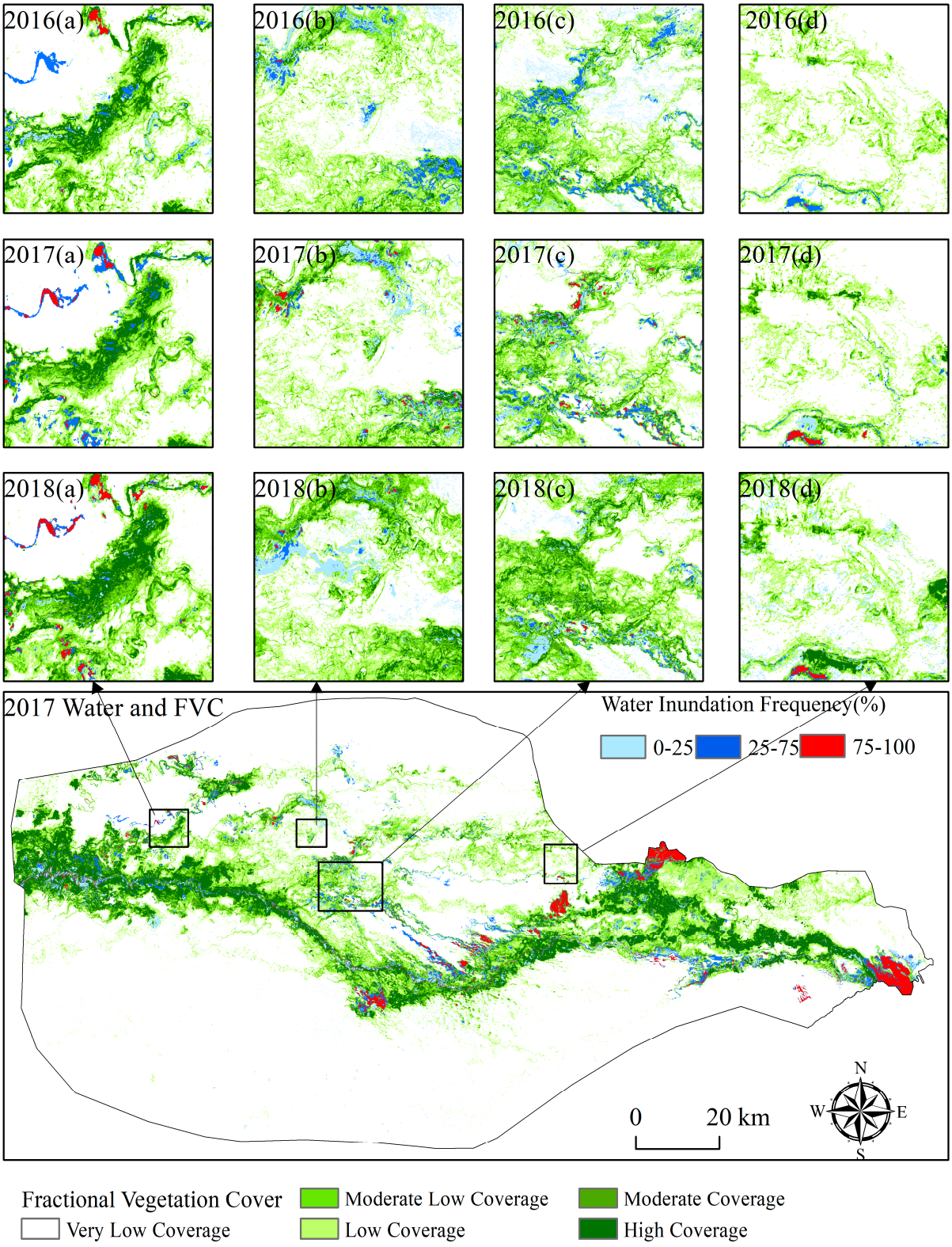

Figure 10. Vegetation FVC in the MROTR remote sensing monitoring area in 2016, 2017 and 2018 (each monitoring area corresponds to the vegetation FVC of the year and the surface waterbody of the year).

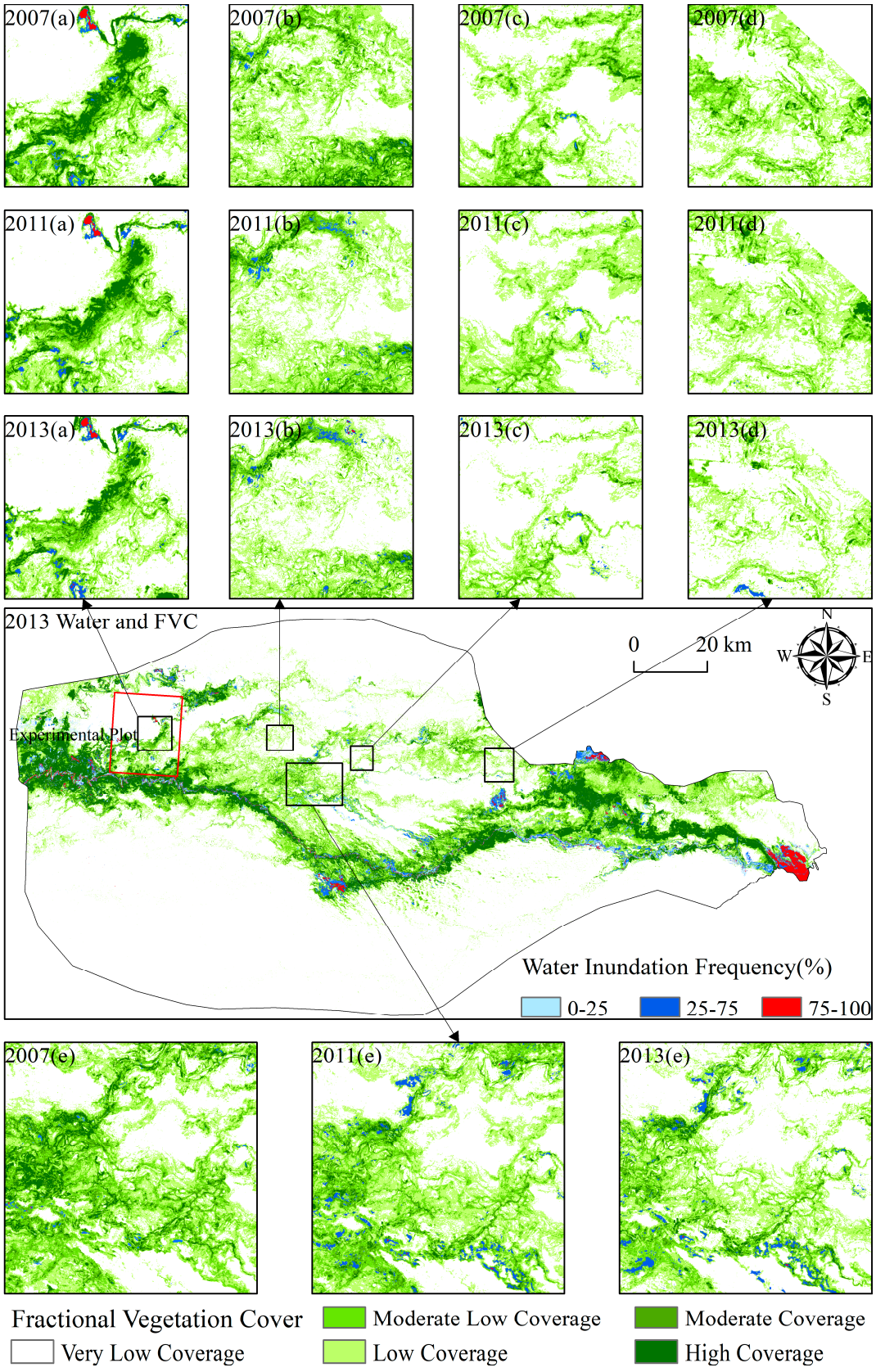

Figure 11. Vegetation FVC in the MROTR remote sensing monitoring areas in 2007, 2011, and 2013. Each monitoring area corresponds to the vegetation FVC of the current year and the surface waterbody of the previous year, e.g., Figure 2007a shows the vegetation FVC of 2007 and the surface waterbody of 2006.

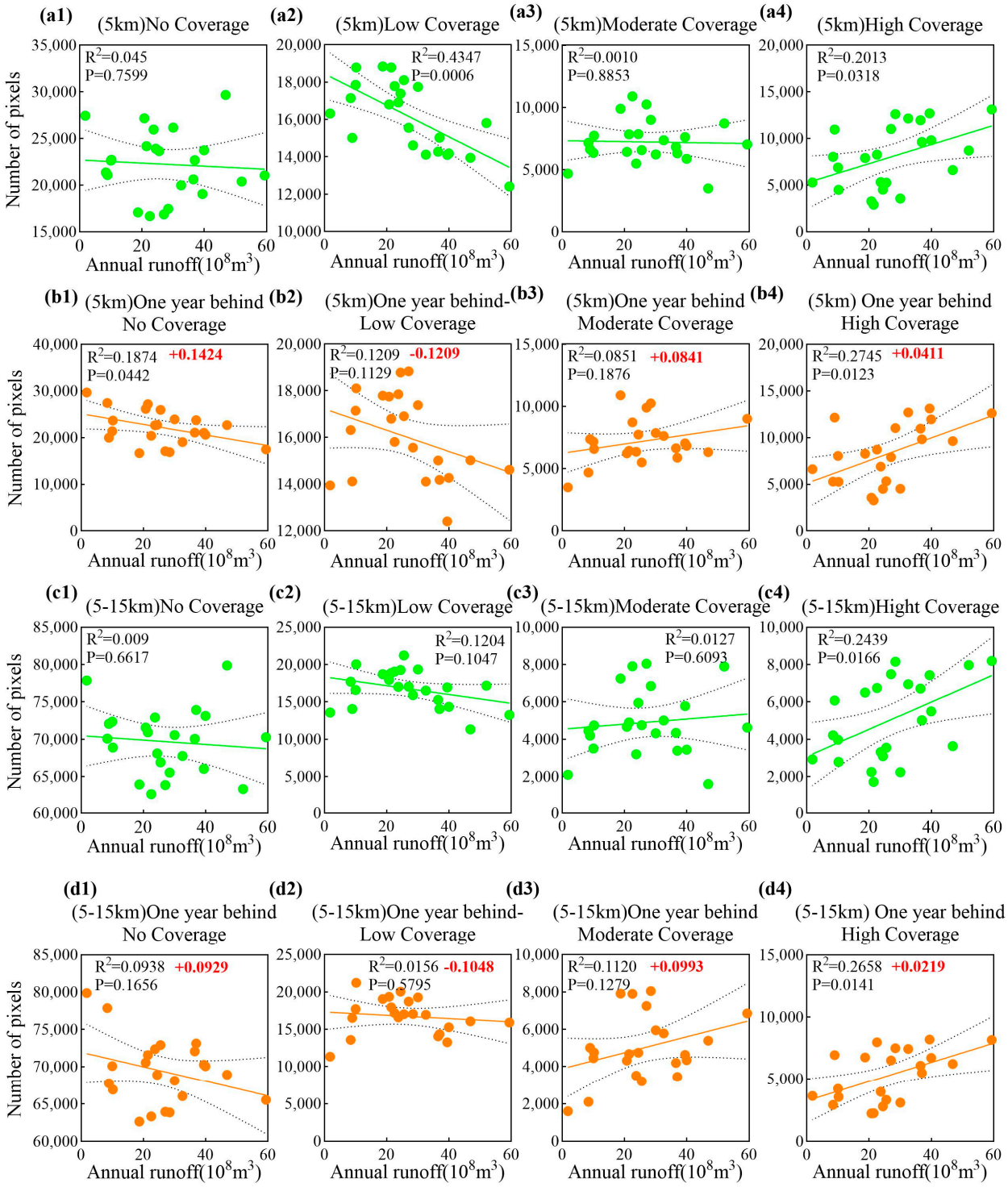

Figure 12. Correlations between water inflows and vegetation cover from 1990 to 2022. (**a**,**b**) show the correlations between different water inflows and vegetation cover within 5 km of the riverbank, (**c**,**d**) show the correlations between water inflows and vegetation cover within 5 km–15 km from the riverbank. (**b**,**d**) show the correlations between water inflows and vegetation cover 1 year after the lag year.

However, the opposite pattern was observed for low vegetation cover. The correlation between river inflow and the same year's vegetation cover was stronger, with weaker correlations for the subsequent year's vegetation, as shown by the decreased R^2 values of −0.1209 and −0.1048 (Figure 12b2,d2). According to previous research [54], deep-rooted

species, such as *Populus euphratica*, and salt-tolerant plants, such as *Tamarix* spp., tend to be influenced more by groundwater levels and long-term water infiltration. The growth of these plants is dependent on water conditions over multiple years. In contrast, low vegetation cover types, which mainly consist of shallow-rooted grasses and shrubs, such as *Suaeda* spp. and *Calligonum* spp., are more responsive to surface water and soil moisture, resulting in a stronger reaction to annual precipitation and water inflow. These species have relatively short life cycles, with water availability quickly reflected in the same year's vegetation cover and growth patterns. These variations highlight the different water-use adaptations and ecological functions of diverse plants in the region.

3.3.3. Correlations of Vegetation Indicators with SWA

From 1990 to 2022, the spatial trend of vegetation cover in the MROTR showed a decreasing pattern, whereas the NDVI time series for the middle reaches and the four subregions exhibited an increasing trend from 2000 to 2022. The SOS showed an advancing trend, and the EOS mostly showed a delaying trend, resulting in an extended growing period. A long-term correlation analysis between the SWA and the vegetation NDVI, SOS, EOS, and growing season length (GLS) revealed that the SWA was positively correlated with the NDVI and negatively correlated with the SOS, EOS, and GLS. The EOS was significantly positively correlated with the duration of the growing season (Figure 13).

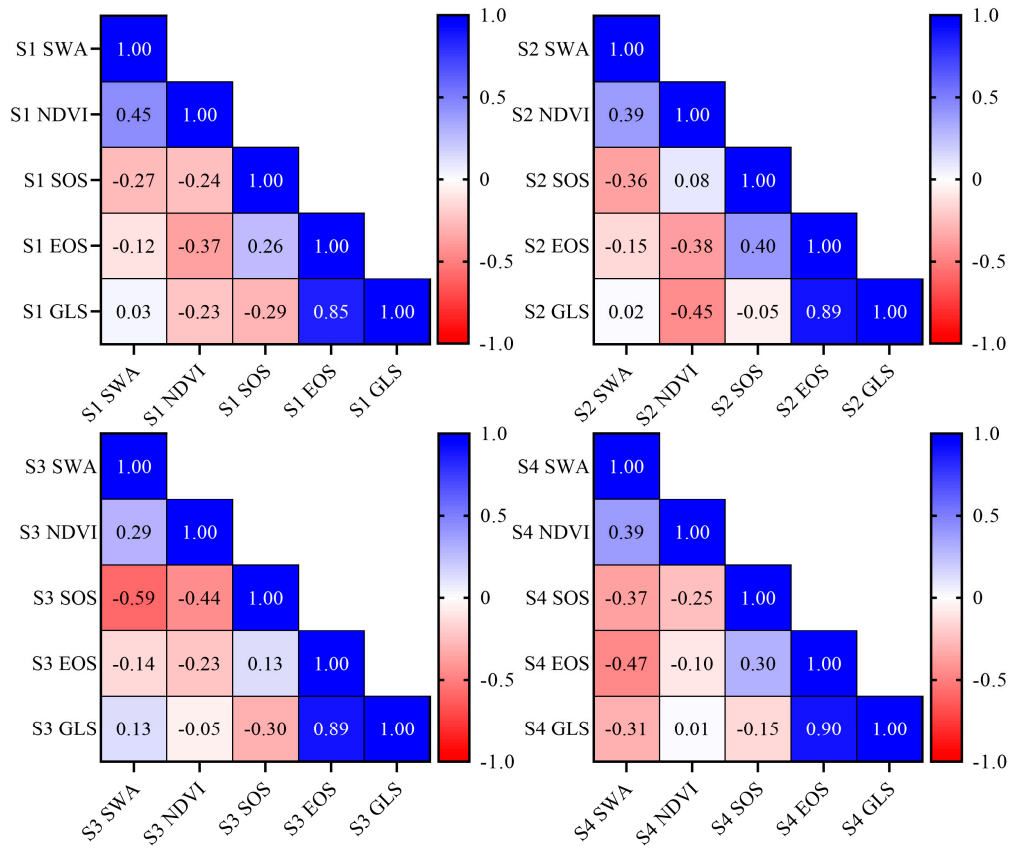

Figure 13. Correlations between surface water area and annual vegetation characteristics.

4. Discussion

4.1. Impact of Ecological Sluice Gate Water Control on Water Bodies

The main objective of using ecological gates for irrigation management in the Tarim River Basin is to enhance water flow to downstream areas, improve conditions for water supply, and work towards the protection and restoration of natural vegetation in regulated areas [28]. In arid regions, the core challenge of ecological conservation lies in how to achieve the optimal match between ecological water supply [55,56] and vegetation water

demand through precise water regulation [57]. As a result, the use of ecological gate systems for water transfer offers a distinct strategy for allocating water resources and facilitating ecological restoration in the Tarim River Basin [58]. Given that its operational mechanism depends on the movement and spatial distribution of water resources within the zones of ecological management, understanding the response patterns of SWA during the EGCW phase is crucial for ecological regulation and accurate regional delineation in the Tarim River Basin.

During the EGCW phase, the SWA in the MROTR significantly increased and exhibited notable spatiotemporal variation (Figure 4). Compared with earlier stages, the expansion of the SWA during the EGCW phase was more stable and rapid, especially in wet years, when the water distribution range expanded significantly (Figure 6). During this period, the regulation by ecological gates reduced ineffective overflow in areas close to the riverbank (2–8 km) and facilitated the lateral transfer of water to farther regions (10–40 km). In both normal and wet years, the SWA continued to increase within the 23–35-km range, with water transfer distances reaching 40 km, thus greatly expanding the distribution of seasonal water bodies. In regions far from the river that are ecologically sensitive, diverting water via ecological gates sets the stage for overflow, thereby encouraging substantial seedling growth [59]. Long-distance water transfer effectively facilitates seed dispersal into new soils and ecosystems, thus expanding the distribution range of plant populations [26,60] demonstrated that surface water inundation is a key driver of vegetation expansion, as the vegetation area significantly increases with the expansion of surface water when groundwater levels are stable. This effective water resource regulation provides the necessary water supply for riparian vegetation growth and improves the conditions for ecological restoration. The area of permanent water bodies remains relatively stable, and the expansion of seasonal water bodies is the main contributor to the increase in the SWA. Additionally, seasonal water bodies are a key factor that influences the distribution of plant species in arid regions [61]. By combining runoff peaks with the expansion of seasonal water bodies, the ecological gate system optimizes water flow regulation, enhances water resource use efficiency, and provides a stable water supply during the vegetation growing season. This regulation strategy during the EGCW phase significantly improves ecological restoration in the MROTR and provides practical insights for future water resource management.

This study significantly contributes to water resource management in arid regions. Bwambale et al. [62] research presents advanced smart monitoring and control strategies for irrigation scheduling, stressing the necessity of precise water regulation mechanisms. Our findings underscore the unique adaptive strategies used in the Tarim River Basin, particularly concerning ecological gate management, which may provide valuable insights for similar global efforts. Observed patterns of surface water expansion and vegetation response highlight both the effectiveness of our approach and the importance of sustainable local ecological management. The construction of ecological gates has modified water distribution, and appropriate flow management can facilitate the expansion of seasonal water bodies and improve vegetation cover. Water resource regulation is ecologically crucial in arid regions, with long-term consequences affecting water availability, vegetation dynamics, and aquatic ecosystem stability. Therefore, implementing water resource regulation requires a comprehensive consideration of the ecological environment's carrying capacity, and strategies should be scientifically formulated to ensure sustainable water use and ecosystem restoration and protection.

4.2. Impact of Ecological Gate-Controlled Water on Desert Riparian Vegetation

In arid regions, water resources serve as the crucial abiotic factor influencing riparian forest ecosystems. The accumulation of ecological water sources, including groundwater, surface water, and soil moisture, effectively promotes vegetation growth [26,63]. According to the FVC trend chart (Figure 8), from 2000 to 2010, vegetation on the northern bank of the MROTR decreased significantly, while from 2010 to 2022, the vegetation on the northern bank increased substantially. This corresponds with the establishment of ecological sluice

and the EGCW phase. The construction phase reduced water overflow from river channels, which caused significant degradation of vegetation on the northern bank of the MROTR. After the completion of the ecological gates and water control embankments, the vegetation on the northern bank increased dramatically.

Our study also reveals that SWA was significantly negatively correlated with low-coverage vegetation within 15 km of the river channel (Figure 12a2,b2,c2,d2). Low-coverage vegetation was more influenced by water bodies in the same year, as shown in Figure 12b2,d2, where the correlation between water bodies and vegetation weakened when there was a 1-year lag. These low-coverage vegetation types, mainly grasses and shrubs [64], such as *Suaeda* spp. and *Calligonum* spp., typically have shallow root systems and are highly dependent on surface water and topsoil moisture [65,66]. These plants often respond strongly to annual precipitation, river replenishment, and surface water expansion, as their short growth cycles cause water fluctuations to be rapidly reflected in the vegetation cover and growth conditions in the same year [67]. As the river flow increases, the SWA expands, which increases the moisture content of the shallow soil and provides a favorable environment for seed germination. However, due to strong evaporation, salinization becomes severe, and the increased water volume washes surface salts into one area. During this period of high soil salinity, it becomes difficult for seedlings to transition to young forests [68–70], resulting in a decline in low-coverage vegetation during this phase. In contrast, SWA promotes the growth of medium- and high-coverage vegetation, with a lag effect that extends as water volumes increase (Figure 12). The varying river flow volumes have significant effects on vegetation at different distances from the river, and they promote the growth of medium- and high-coverage vegetation types. Medium- and high-coverage vegetation are composed mainly of deep-rooted plants, such as *Populus euphratica* [71] and salt-tolerant species, such as *Tamarix* spp. [64]. Since their roots can penetrate deep into the ground and adapt to dry and saline-alkaline soil conditions [72,73], their growth is often influenced by groundwater levels and long-term water infiltration. Therefore, their growth trends are more dependent on water conditions from previous years, which explains why medium- and high-coverage vegetation are more affected by the previous year's waterbodies than by the current year's waterbodies.

The effectiveness of water delivery through ecological gates fluctuates with varying water volumes. In wet years, ecological gates can sustain ecological protection and vegetation recovery, whereas in low-flow years, their guaranteed rate of ecological protection and vegetation recovery for desert riparian vegetation is low [25]. Different vegetation types have varying water requirements, and different flooding frequencies have distinct impacts on the species diversity of downstream vegetation in the Tarim River [18]. Too low or too high flooding frequencies are not conducive to restoring and maintaining species diversity, while moderate flooding disturbances can maintain high biodiversity [74]. After flooding in the middle reaches of the Tarim River Basin, the number and diversity of plant species decrease as the distance from the ecological gates increases [61]. After the implementation of EGCW, the area of low-coverage vegetation increased significantly, whereas the declining trends in medium- and high-coverage vegetation types slowed. Ecological water conservancy projects in the Tarim River Basin have enhanced the coupling between the water supply and vegetation water demand, improving the efficiency of water use for plant growth.

4.3. Limitations and Future Prospects of This Study

The accuracy of waterbody extraction is significantly influenced by the quality of the remote sensing data. Because of the 16-day revisit cycle of Landsat, short-term water events (such as flash floods) may be overlooked. Additionally, the 30-m spatial resolution of Landsat imagery may be insufficient to adequately capture the spatial distribution of small waterbodies. In the future, the use of higher-resolution multispectral data (such as Sentinel-2A) and the integration of optical imagery with SAR data could improve the accuracy of waterbody extraction.

This study analyzed the changes in vegetation cover types across different stages, but because of the high heterogeneity of riparian forest vegetation in desert areas, the responses of plants vary. Research has focused primarily on the expansion and seasonal dynamics of surface water. Although surface water promotes vegetation recovery, the long-term effects of groundwater dynamics on plant growth have not been thoroughly explored. Groundwater is crucial for the growth of deep-rooted plants, such as *Populus euphratica* and *Tamarix* spp., in arid regions; however, this aspect was insufficiently analyzed in this study. The effectiveness of EGCW fluctuates significantly in different water years, and the alignment between vegetation recovery and water resource regulation remains uncertain in some regions. Diverse vegetation types exhibit spatial and temporal differences in water demand. Low-coverage vegetation is sensitive to annual waterbody changes, whereas medium- and high-coverage vegetation show delayed responses to water conditions in previous years. This distinction will be a key focus of future research.

5. Conclusions

From 1990 to 2022, the SWA in the MROTR underwent significant changes, particularly after the construction of ecological gates, with a growth rate of 28.8 km^2 per year. The regulation of water resources by the ecological gate system effectively reduced the inefficient spread of water near riverbanks while significantly increasing the water area in more distant regions. This effect was especially pronounced in wet and extremely wet years, where the water delivery distance reached 40 km. Since the implementation of continuous water delivery and the construction of ecological gates in the MROTR in 2001, both the temporal and spatial dynamics of vegetation have shown a significant response. Overall vegetation coverage has become less volatile, and the area of low-coverage vegetation has gradually increased, reflecting the differential impacts of water resource regulation on various vegetation types. During the EGCW stage, the vegetation on the northern bank of the river significantly recovered, whereas the vegetation on southern bank exhibited a declining trend. The lag effect of SWA on vegetation growth indicates that deep-rooted plants are sensitive to long-term water level changes, while low-coverage vegetation responds more directly to water changes within the same year. These findings demonstrate that ecological gates have played a critical role in improving water resource efficiency and promoting regional ecological restoration.

Author Contributions: Conceptualization, J.W.; Methodology, J.W.; Software, J.W.; Validation, B.H., F.S. and K.L.; Formal analysis, Q.Z.; Investigation, J.W.; Resources, J.W.; Data curation, H.X.; Writing—original draft preparation, J.W.; Writing—review and editing, F.G.; Visualization, J.W.; Supervision, B.H.; Project administration, F.S.; Funding acquisition, F.G. and H.X. All authors have read and agreed to the published version of the manuscript.

Funding: This research was funded by [Major Scientific and Technological Special Project of the Xinjiang Uygur Autonomous Region] grant number [Grant number 2023A02002], and the APC was funded by [Fan Gao and Hailiang Xu].

Data Availability Statement: The original contributions presented in this study are included in the article. Further inquiries can be directed to the corresponding author(s).

Conflicts of Interest: The authors declare no conflict of interest.

References

1. Deng, Y.; Jiang, W.; Ye, X.; Zhang, L.; Jia, K. Water Occurrence in the Two Largest Lakes in China Based on Long-Term Landsat Images: Spatiotemporal Changes, Ecological Impacts, and Influencing Factors. *Remote Sens.* **2022**, *14*, 3875. [CrossRef]
2. Rassam, D.W.; Peeters, L.; Pickett, T.; Jolly, I.; Holz, L. Accounting for Surface–Groundwater Interactions and Their Uncertainty in River and Groundwater Models: A Case Study in the Namoi River, Australia. *Environ. Model. Softw.* **2013**, *50*, 108–119. [CrossRef]
3. Yu, J.; Rong, Y.; Lin, Y.; Li, X.; Gao, C.; Zhang, T.; Zhou, X.; Cai, J.; Sneeuw, N. Spatiotemporal Dynamic Impacts of Lake Victoria Water Volume Variations on Sustainable Economic Development. *Int. J. Appl. Earth Obs. Geoinf.* **2023**, *123*, 103475. [CrossRef]
4. Hao, X.; Chen, Y.; Xu, C.; Li, W. Impacts of Climate Change and Human Activities on the Surface Runoff in the Tarim River Basin over the Last Fifty Years. *Water Resour. Manag.* **2008**, *22*, 1159–1171. [CrossRef]

5. Guo, L.; Shan, N.; Zhang, Y.; Sun, F.; Liu, W.; Shi, Z.; Zhang, Q. Separating the Effects of Climate Change and Human Activity on Water Use Efficiency over the Beijing-Tianjin Sand Source Region of China. *Sci. Total Environ.* **2019**, *690*, 584–595. [CrossRef]
6. Li, Q.; Liu, Z.; Yang, Y.; Han, Y.; Wang, X. Evaluation of Water Resources Carrying Capacity in Tarim River Basin under Game Theory Combination Weights. *Ecol. Indic.* **2023**, *154*, 110609. [CrossRef]
7. Günen, M.A.; Atasever, U.H. Remote Sensing and Monitoring of Water Resources: A Comparative Study of Different Indices and Thresholding Methods. *Sci. Total Environ.* **2024**, *926*, 172117. [CrossRef]
8. McFeeters, S.K. The Use of the Normalized Difference Water Index (NDWI) in the Delineation of Open Water Features. *Int. J. Remote Sens.* **1996**, *17*, 1425–1432. [CrossRef]
9. Xu, H. Modification of Normalised Difference Water Index (NDWI) to Enhance Open Water Features in Remotely Sensed Imagery. *Int. J. Remote Sens.* **2006**, *27*, 3025–3033. [CrossRef]
10. Zou, Z.; Dong, J.; Menarguez, M.A.; Xiao, X.; Qin, Y.; Doughty, R.B.; Hooker, K.V.; David Hambright, K. Continued Decrease of Open Surface Water Body Area in Oklahoma during 1984–2015. *Sci. Total Environ.* **2017**, *595*, 451–460. [CrossRef]
11. Zhou, Y.; Dong, J.; Xiao, X.; Liu, R.; Zou, Z.; Zhao, G.; Ge, Q. Continuous Monitoring of Lake Dynamics on the Mongolian Plateau Using All Available Landsat Imagery and Google Earth Engine. *Sci. Total Environ.* **2019**, *689*, 366–380. [CrossRef] [PubMed]
12. Amani, M.; Ghorbanian, A.; Ahmadi, S.A.; Kakooei, M.; Moghimi, A.; Mirmazloumi, S.M.; Moghaddam, S.H.A.; Mahdavi, S.; Ghahremanloo, M.; Parsian, S.; et al. Google Earth Engine Cloud Computing Platform for Remote Sensing Big Data Applications: A Comprehensive Review. *IEEE J. Sel. Top. Appl. Earth Obs. Remote Sens.* **2020**, *13*, 5326–5350. [CrossRef]
13. Zhao, Q.; Yu, L.; Li, X.; Peng, D.; Zhang, Y.; Gong, P. Progress and Trends in the Application of Google Earth and Google Earth Engine. *Remote Sens.* **2021**, *13*, 3778. [CrossRef]
14. Chen, Z.; Zhao, S. Automatic Monitoring of Surface Water Dynamics Using Sentinel-1 and Sentinel-2 Data with Google Earth Engine. *Int. J. Appl. Earth Obs. Geoinf.* **2022**, *113*, 103010. [CrossRef]
15. Jin, H.; Fang, S.; Chen, C. Mapping of the Spatial Scope and Water Quality of Surface Water Based on the Google Earth Engine Cloud Platform and Landsat Time Series. *Remote Sens.* **2023**, *15*, 4986. [CrossRef]
16. Pekel, J.-F.; Cottam, A.; Gorelick, N.; Belward, A.S. High-Resolution Mapping of Global Surface Water and Its Long-Term Changes. *Nature* **2016**, *540*, 418–422. [CrossRef]
17. Zou, Z.; Xiao, X.; Dong, J.; Qin, Y.; Doughty, R.B.; Menarguez, M.A.; Zhang, G.; Wang, J. Divergent Trends of Open-Surface Water Body Area in the Contiguous United States from 1984 to 2016. *Proc. Natl. Acad. Sci. USA* **2018**, *115*, 3810–3815. [CrossRef]
18. Xu, H.; Ye, M.; Li, J. The Ecological Characteristics of the Riparian Vegetation Affected by River Overflowing Disturbance in the Lower Tarim River. *Environ. Geol.* **2009**, *58*, 1749–1755. [CrossRef]
19. Jiao, A.; Wang, W.; Ling, H.; Deng, X.; Yan, J.; Chen, F. Effect Evaluation of Ecological Water Conveyance in Tarim River Basin, China. *Front. Environ. Sci.* **2022**, *10*, 1019695. [CrossRef]
20. Ye, Z.; Chen, Y.; Li, W.; Yan, Y. Effect of the Ecological Water Conveyance Project on Environment in the Lower Tarim River, Xinjiang, China. *Environ. Monit. Assess.* **2009**, *149*, 9–17. [CrossRef]
21. Li, M.; Deng, M.; Ling, H.; Xu, J. Development of a New Rotational Irrigation Model in an Arid Basin Based on Ecological Zoning and Sluice Regulation. *Agric. Water Manag.* **2024**, *296*, 108800. [CrossRef]
22. Yu, Y.; Yu, R.; Chen, X.; Yu, G.; Gan, M.; Disse, M. Agricultural Water Allocation Strategies along the Oasis of Tarim River in Northwest China. *Agric. Water Manag.* **2017**, *187*, 24–36. [CrossRef]
23. Lin, J.; Chen, Q. Analyzing and Simulating the Influence of a Water Conveyance Project on Land Use Conditions in the Tarim River Region. *Land* **2023**, *12*, 2073. [CrossRef]
24. Moreno, M.; Ortiz, P.; Ortiz, R. Analysis of the Impact of Green Urban Areas in Historic Fortified Cities Using Landsat Historical Series and Normalized Difference Indices. *Sci. Rep.* **2023**, *13*, 8982. [CrossRef]
25. Wu, J.; Gao, F.; Xu, H.; He, B.; Liu, K. Dynamic Monitoring of Open-Surface Water Bodies in the Middle Reaches of the Tarim River Based on the GEE Cloud Platform. *AQUA Water Infrastruct. Ecosyst. Soc.* **2024**, *73*, jws2024233. [CrossRef]
26. Song, J.; Betz, F.; Aishan, T.; Halik, Ü.; Abliz, A. Impact of Water Supply on the Restoration of the Severely Damaged Riparian Plants along the Tarim River in Xinjiang, Northwest China. *Ecol. Indic.* **2024**, *158*, 111570. [CrossRef]
27. Ye, Z.; Chen, S.; Zhang, Q.; Liu, Y.; Zhou, H. Ecological Water Demand of Taitema Lake in the Lower Reaches of the Tarim River and the Cherchen River. *Remote Sens.* **2022**, *14*, 832. [CrossRef]
28. Qian, K.; Ma, X.; Yan, W.; Li, J.; Xu, S.; Liu, Y.; Luo, C.; Yu, W.; Yu, X.; Wang, Y.; et al. Trade-Offs and Synergies among Ecosystem Services in Inland River Basins under the Influence of Ecological Water Transfer Project: A Case Study on the Tarim River Basin. *Sci. Total Environ.* **2024**, *908*, 168248. [CrossRef]
29. Li, W.; Huang, F.; Shi, F.; Wei, X.; Zamanian, K.; Zhao, X. Human and Climatic Drivers of Land and Water Use from 1997 to 2019 in Tarim River Basin, China. *Int. Soil Water Conserv. Res.* **2021**, *9*, 532–543. [CrossRef]
30. Ståhl, G.; Ekström, M.; Dahlgren, J.; Esseen, P.; Grafström, A.; Jonsson, B. Presence–Absence Sampling for Estimating Plant Density Using Survey Data with Variable Plot Size. *Methods Ecol. Evol.* **2020**, *11*, 580–590. [CrossRef]
31. Arfa, A.; Minaei, M. Utilizing Multitemporal Indices and Spectral Bands of Sentinel-2 to Enhance Land Use and Land Cover Classification with Random Forest and Support Vector Machine. *Adv. Space Res.* **2024**. [CrossRef]
32. Huete, A.R.; Jackson, R.D. Suitability of Spectral Indices for Evaluating Vegetation Characteristics on Arid Rangelands. *Remote Sens. Environ.* **1987**, *23*, 213-IN8. [CrossRef]

33. Waring, R.H.; Coops, N.C.; Fan, W.; Nightingale, J.M. MODIS Enhanced Vegetation Index Predicts Tree Species Richness across Forested Ecoregions in the Contiguous U.S.A. *Remote Sens. Environ.* **2006**, *103*, 218–226. [CrossRef]
34. Lu, H.; Zhao, R.; Zhao, L.; Lyu, B.; Wang, J.; Zhang, L. A Contrarian Growth: The Spatiotemporal Dynamics of Open-Surface Water Bodies on the Northern Slope of Kunlun Mountains. *Ecol. Indic.* **2023**, *157*, 111249. [CrossRef]
35. Zhao, Z.; Li, H.; Song, X.; Sun, W. Dynamic Monitoring of Surface Water Bodies and Their Influencing Factors in the Yellow River Basin. *Remote Sens.* **2023**, *15*, 5157. [CrossRef]
36. Liu, Y.; Xiao, X.; Li, J.; Wang, X.; Chen, B.; Sun, C.; Wang, J.; Tian, P.; Zhang, H. Tracking Changes in Coastal Land Cover in the Yellow Sea, East Asia, Using Sentinel-1 and Sentinel-2 Time-Series Images and Google Earth Engine. *ISPRS J. Photogramm. Remote Sens.* **2023**, *196*, 429–444. [CrossRef]
37. Chen, X.; Zhao, X.; Zhao, Y.; Wang, R.; Lu, J.; Zhuang, H.; Bai, L. Interaction of Climate Change and Anthropogenic Activity on the Spatiotemporal Changes of Surface Water Area in Horqin Sandy Land, China. *Remote Sens.* **2023**, *15*, 1918. [CrossRef]
38. Yamazaki, D.; Trigg, M.A.; Ikeshima, D. Development of a Global ~90 m Water Body Map Using Multi-Temporal Landsat Images. *Remote Sens. Environ.* **2015**, *171*, 337–351. [CrossRef]
39. Jiang, H.; Chen, A.; Wu, Y.; Zhang, C.; Chi, Z.; Li, M.; Wang, X. Vegetation Monitoring for Mountainous Regions Using a New Integrated Topographic Correction (ITC) of the SCS + C Correction and the Shadow-Eliminated Vegetation Index. *Remote Sens.* **2022**, *14*, 3073. [CrossRef]
40. Lu, S.; Wu, B.; Yan, N.; Wang, H. Water Body Mapping Method with HJ-1A/B Satellite Imagery. *Int. J. Appl. Earth Obs. Geoinf.* **2011**, *13*, 428–434. [CrossRef]
41. Zhang, X.; Liu, L.; Wang, Y.; Hu, Y.; Zhang, B. A SPECLib-Based Operational Classification Approach: A Preliminary Test on China Land Cover Mapping at 30 m. *Int. J. Appl. Earth Obs. Geoinf.* **2018**, *71*, 83–94. [CrossRef]
42. Deng, X.; Song, C.; Liu, K.; Ke, L.; Zhang, W.; Ma, R.; Zhu, J.; Wu, Q. Remote Sensing Estimation of Catchment-Scale Reservoir Water Impoundment in the Upper Yellow River and Implications for River Discharge Alteration. *J. Hydrol.* **2020**, *585*, 124791. [CrossRef]
43. Li, X.; Zhou, Y.; Meng, L.; Asrar, G.R.; Lu, C.; Wu, Q. A Dataset of 30 m Annual Vegetation Phenology Indicators (1985–2015) in Urban Areas of the Conterminous United States. *Earth Syst. Sci. Data* **2019**, *11*, 881–894. [CrossRef]
44. Li, X.; Zhou, Y.; Asrar, G.R.; Mao, J.; Li, X.; Li, W. Response of Vegetation Phenology to Urbanization in the Conterminous United States. *Glob. Change Biol.* **2017**, *23*, 2818–2830. [CrossRef] [PubMed]
45. Sen, P.K. Estimates of the Regression Coefficient Based on Kendall's Tau. *J. Am. Stat. Assoc.* **1968**, *63*, 1379–1389. [CrossRef]
46. Li, C.; Wang, R.; Cui, X.; Wu, F.; Yan, Y.; Peng, Q.; Qian, Z.; Xu, Y. Responses of Vegetation Spring Phenology to Climatic Factors in Xinjiang, China. *Ecol. Indic.* **2021**, *124*, 107286. [CrossRef]
47. Mann, H.B. Nonparametric Tests against Trend. *Econometrica* **1945**, *13*, 245–259. [CrossRef]
48. Mudelsee, M. Trend Analysis of Climate Time Series: A Review of Methods. *Earth Sci. Rev.* **2019**, *190*, 310–322. [CrossRef]
49. Behdani, Z.; Darehmiraki, M. Theil-Sen Estimators for Fuzzy Regression Model. *Iran. J. Fuzzy Syst.* **2024**, *21*, 177–192. [CrossRef]
50. Wang, F.; Shao, W.; Yu, H.; Kan, G.; He, X.; Zhang, D.; Ren, M.; Wang, G. Re-Evaluation of the Power of the Mann-Kendall Test for Detecting Monotonic Trends in Hydrometeorological Time Series. *Front. Earth Sci.* **2020**, *8*, 14. [CrossRef]
51. Asfaw, A.; Simane, B.; Hassen, A.; Bantider, A. Variability and Time Series Trend Analysis of Rainfall and Temperature in Northcentral Ethiopia: A Case Study in Woleka Sub-Basin. *Weather Clim. Extrem.* **2018**, *19*, 29–41. [CrossRef]
52. Yang, H.; Yu, J.; Xu, W.; Wu, Y.; Lei, X.; Ye, J.; Geng, J.; Ding, Z. Long-Time Series Ecological Environment Quality Monitoring and Cause Analysis in the Dianchi Lake Basin, China. *Ecol. Indic.* **2023**, *148*, 110084. [CrossRef]
53. Rebekić, A.; Lončarić, Z.; Petrović, S.; Marić, S. Pearson's or Spearman's Correlation Coefficient—Which One to Use? *Poljoprivreda* **2015**, *21*, 47–54. [CrossRef]
54. Zhang, Y.; Chen, Y.; Zhang, D. Quantitative Classification and Analysis on Plant Communities in the Middle Reaches of the Tarim River. *J. Geogr. Sci.* **2003**, *13*, 225–232. [CrossRef]
55. Cosgrove, W.J.; Loucks, D.P. Water Management: Current and Future Challenges and Research Directions. *Water Resour. Res.* **2015**, *51*, 4823–4839. [CrossRef]
56. Hering, D.; Borja, A.; Carstensen, J.; Carvalho, L.; Elliott, M.; Feld, C.K.; Heiskanen, A.-S.; Johnson, R.K.; Moe, J.; Pont, D.; et al. The European Water Framework Directive at the Age of 10: A Critical Review of the Achievements with Recommendations for the Future. *Sci. Total Environ.* **2010**, *408*, 4007–4019. [CrossRef]
57. Wang, W.; Han, F.; Kong, Z.; Ling, H.; Hao, X. The Maximum Threshold of Vegetation Restoration (EVI-Area) in Typical Watersheds of Arid Regions under Water Constraints. *Ecol. Indic.* **2024**, *158*, 111580. [CrossRef]
58. Yan, D.; Chen, L.; Sun, H.; Liao, W.; Chen, H.; Wei, G.; Zhang, W.; Tuo, Y. Allocation of Ecological Water Rights Considering Ecological Networks in Arid Watersheds: A Framework and Case Study of Tarim River Basin. *Agric. Water Manag.* **2022**, *267*, 107636. [CrossRef]
59. Ling, H.; Zhang, P.; Xu, H.; Zhang, G. Determining the Ecological Water Allocation in a Hyper-Arid Catchment with Increasing Competition for Water Resources. *Glob. Planet. Chang.* **2016**, *145*, 143–152. [CrossRef]
60. Al-Munqedhi, B.M.; El-Sheikh, M.A.; Alfarhan, A.H.; Alkahtani, A.M.; Arif, I.A.; Rajagopal, R.; Alharthi, S.T. Climate Change and Hydrological Regime in Arid Lands: Impacts of Dams on the Plant Diversity, Vegetation Structure and Soil in Saudi Arabia. *Saudi J. Biol. Sci.* **2022**, *29*, 3194–3206. [CrossRef]

61. Wang, Y.; Li, J.; Qian, K.; Ye, M. Response of Plant Species Diversity to Flood Irrigation in the Tarim River Basin, Northwest China. *Sustainability* **2023**, *15*, 1243. [CrossRef]
62. Bwambale, E.; Abagale, F.K.; Anornu, G.K. Smart Irrigation Monitoring and Control Strategies for Improving Water Use Efficiency in Precision Agriculture: A Review. *Agric. Water Manag.* **2022**, *260*, 107324. [CrossRef]
63. Mohtaram, A.; Shafizadeh-Moghadam, H.; Ketabchi, H. Reconstruction of Total Water Storage Anomalies from GRACE Data Using the LightGBM Algorithm with Hydroclimatic and Environmental Covariates. *Groundw. Sustain. Dev.* **2024**, *26*, 101260. [CrossRef]
64. Zhang, Y.M.; Chen, Y.N.; Pan, B.R. Distribution and Floristics of Desert Plant Communities in the Lower Reaches of Tarim River, Southern Xinjiang, People's Republic of China. *J. Arid Environ.* **2005**, *63*, 772–784. [CrossRef]
65. Bucci, S.J.; Scholz, F.G.; Goldstein, G.; Meinzer, F.C.; Arce, M.E. Soil Water Availability and Rooting Depth as Determinants of Hydraulic Architecture of Patagonian Woody Species. *Oecologia* **2009**, *160*, 631–641. [CrossRef]
66. Schenk, H.J.; Jackson, R.B. Rooting Depths, Lateral Root Spreads and below-Ground/above-Ground Allometries of Plants in Water-Limited Ecosystems. *J. Ecol.* **2002**, *90*, 480–494. [CrossRef]
67. Zeng, Y.; Zhao, C.; Li, J.; Li, Y.; Lv, G.; Liu, T. Effect of Groundwater Depth on Riparian Plant Diversity along Riverside-Desert Gradients in the Tarim River. *J. Plant Ecol.* **2019**, *12*, 564–573. [CrossRef]
68. Nosetto, M.D.; Jobbágy, E.G.; Tóth, T.; Di Bella, C.M. The Effects of Tree Establishment on Water and Salt Dynamics in Naturally Salt-Affected Grasslands. *Oecologia* **2007**, *152*, 695–705. [CrossRef]
69. Weisbrod, N.; Nativh, R.; Adar, K.M.; Ronend, D. Salt Accumulation and Flushing in Unsaturated Fractures in an Arid Environment. *Groundwater* **2000**, *38*, 452–461. [CrossRef]
70. Xin, P.; Wilson, A.; Shen, C.; Ge, Z.; Moffett, K.B.; Santos, I.R.; Chen, X.; Xu, X.; Yau, Y.Y.Y.; Moore, W.; et al. Surface Water and Groundwater Interactions in Salt Marshes and Their Impact on Plant Ecology and Coastal Biogeochemistry. *Rev. Geophys.* **2022**, *60*, e2021RG000740. [CrossRef]
71. Keram, A.; Halik, Ü.; Aishan, T.; Keyimu, M.; Jiapaer, K.; Li, G. Tree Mortality and Regeneration of Euphrates Poplar Riparian Forests along the Tarim River, Northwest China. *For. Ecosyst.* **2021**, *8*, 49. [CrossRef]
72. Hayward, H.E.; Wadleigh, C.H. Plant Growth on Saline and Alkali Soils*. In *Advances in Agronomy*; Norman, A.G., Ed.; Academic Press: Cambridge, MA, USA, 1949; Volume 1, pp. 1–38.
73. Sun, J.; Zhao, X.; Fang, Y.; Gao, F.; Wu, C.; Xia, J. Effects of Water and Salt for Groundwater-Soil Systems on Root Growth and Architecture of Tamarix Chinensis in the Yellow River Delta, China. *J. For. Res.* **2023**, *34*, 441–452. [CrossRef]
74. Chen, Y.-N.; Zilliacus, H.; Li, W.-H.; Zhang, H.-F.; Chen, Y.-P. Ground-Water Level Affects Plant Species Diversity along the Lower Reaches of the Tarim River, Western China. *J. Arid Environ.* **2006**, *66*, 231–246. [CrossRef]